nature

https://doi.org/10.1038/s41586-023-06869-w

Accelerated Article Preview

Phages overcome bacterial immunity via diverse anti-defence proteins

Received: 1 May 2023

Accepted: 14 November 2023

Accelerated Article Preview

Cite this article as: Yirmiya, E. et al. Phages overcome bacterial immunity via diverse anti-defence proteins. *Nature* https://doi.org/10.1038/s41586-023-06869-w (2023)

Erez Yirmiya, Azita Leavitt, Allen Lu, Adelyn E. Ragucci, Carmel Avraham, Ilya Osterman, Jeremy Garb, Sadie P. Antine, Sarah E. Mooney, Samuel J. Hobbs, Philip J. Kranzusch, Gil Amitai & Rotem Sorek

Phages overcome bacterial immunity via diverse anti-defence proteins

Erez Yirmiya[1,#], Azita Leavitt[1,#] , Allen Lu[2,3], Adelyn E. Ragucci[2,3], Carmel Avraham[1], Ilya Osterman[1], Jeremy Garb[1], Sadie P. Antine[2,3], Sarah E. Mooney[2,3], Samuel J. Hobbs[2,3], Philip J. Kranzusch[2,3,4], Gil Amitai[1,*], Rotem Sorek[1,*]

[1]Department of Molecular Genetics, Weizmann Institute of Science, Rehovot 7610001, Israel

[2]Department of Microbiology, Harvard Medical School, Boston, MA, USA

[3]Department of Cancer Immunology and Virology, Dana-Farber Cancer Institute, Boston, MA, USA

[4]Parker Institute for Cancer Immunotherapy at Dana-Farber Cancer Institute, Boston, MA, USA

[#] These authors contributed equally to this work

[*]correspondence: gil.amitai@weizmann.ac.il , rotem.sorek@weizmann.ac.il

Summary paragraph

It was recently shown that bacteria employ, apart from CRISPR-Cas and restriction systems, a considerable diversity of phage resistance systems[1–4], but it is largely unknown how phages cope with this multilayered bacterial immunity. Here, we analyzed groups of closely related *Bacillus* phages that showed differential sensitivity to bacterial defense systems, and discovered four distinct families of anti-defense proteins that inhibit the Gabija, Thoeris, and Hachiman systems. We show that these proteins Gad1, Gad2, Tad2, and Had1 efficiently cancel the defensive activity when co-expressed with the respective defense system or introduced into phage genomes. Homologs of these anti-defense proteins are found in hundreds of phages that infect taxonomically diverse bacterial species. We show that the anti-Gabija protein Gad1 blocks the ability of the Gabija defense complex to cleave phage-derived DNA. Our data further reveal an anti-Thoeris protein, denoted Tad2, which is a "sponge" that sequesters the immune signaling molecules produced by Thoeris TIR-domain proteins in response to phage. Our results demonstrate that phages encode an arsenal of anti-defense proteins that can disable a variety of bacterial defense mechanisms.

Main text

The arms race between bacteria and their viruses has fueled the evolution of defense systems that protect bacteria from phage infection[1–4]. Phages, in return, developed mechanisms that allow them to overcome bacterial defenses[5]. Multiple phages were shown to encode anti-restriction proteins, which inhibit restriction-modification (RM) systems by direct binding to the restriction enzyme[6,7] or by masking restriction sites[8]. Phages are also known to encode many CRISPR-Cas inhibitors, which function via a variety of mechanisms including inhibition of CRISPR RNA loading[9], diversion of the CRISPR-Cas complex to bind non-specific DNA[10], prevention of target DNA binding or cleavage[11], and many additional mechanisms[12–15]. Phage proteins and non-coding RNAs that inhibit toxin-antitoxin-mediated defense have also been described[16,17].

Whereas early research focused on RM and later on CRISPR-Cas as the main mechanisms of defense against phage, recent studies exposed dozens of previously unknown defense systems that are widespread

among bacteria and archaea[2,18–23]. These systems mediate defense by employing a plethora of molecular mechanisms, including small-molecule signaling[20,24–28], production of antiviral compounds[22,29], and reverse transcription of non-coding RNAs[21,30]. Recently, several phage proteins that inhibit the bacterial CBASS and Thoeris defense systems have been described[31–33]. However, it is still mostly unknown whether and how phages can overcome the wide variety of newly reported defense systems. In the current study we use comparative genomics of closely related phages to discover four distinct families of phage proteins that inhibit the Gabija, Thoeris, and Hachiman defense systems.

Identification of anti-defense genes

In a previous study, we demonstrated that analysis of genomically-similar phages that display differential sensitivity to bacterial immunity enabled the discovery of a phage protein, called Tad1, that inhibits the Thoeris defense system[33]. To examine whether this methodology could be used to systematically detect anti-defense proteins within phages, we isolated and analyzed several groups of closely related phages, and tested their sensitivity to multiple defense systems that protect *Bacillus* species from phage infection[18] (fig. 1a). One group included eight newly isolated phages from the SPbeta group, which also includes the previously isolated phages SPbeta, phi3T and SPR[34–36]. These are temperate *Siphoviridae* phages with ~130 kb genomes, with 43–96% alignable genomes when comparing phage pairs from this group (ED fig. 1a, Supplementary tables 1,2). A second group included six phages similar to phage SPO1, a lytic *Myoviridae* phage with a ~130 kb-long genome[37]. Over 85% of the genome was alignable when comparing phage pairs from this group, with high (80–99%) sequence identity in alignable regions (fig. 1b, Supplementary tables 3,4). The third group of phages included eight previously-isolated phages from the SBSphiJ group, which were reported in a recent study[33] (ED fig. 1b, Supplementary tables 5,6).

We next used this set of 25 phages to infect strains of *Bacillus subtilis* that expressed each of the defense systems described in Doron *et al*[18] as protecting against phages in *B. subtilis.* Five of these systems protected against at least one of the phages tested (fig. 1c). However, phages from the same group displayed remarkably different properties when infecting defense-system-containing bacteria. For example, the Gabija defense system provided strong protection against phages SPbeta and SPbetaL8 but not against other phages from the SPbeta group such as SPR and phi3T; and the Hachiman defense system provided defense against all phages of the SBSphiJ group except SBSphiJ4 (fig. 1c).

To identify phage genes that may explain the differential defense phenotype, we analyzed the gene content in groups of phages that overcame each defense system and compared it to the gene content in phages that were blocked by the system. Genes common to phages that overcame the defense system, which were not found in any of the phages that were blocked by the defense system, were considered as candidate anti-defense genes and were further examined experimentally.

Phage genes that inhibit Gabija

Gabija is a widespread bacterial defense system found in >15% of sequenced bacterial and archaeal genomes[39]. This system comprises two genes, *gajA* and *gajB*, which encode a DNA endonuclease and a UvrD-like helicase domain, respectively[18,40]. The Gabija system was shown to provide defense against a diverse set of phages[18,41].

The Gabija system from *Bacillus cereus* VD045, when cloned within *B. subtilis*, provided strong protection against some phages of the SPbeta group including SPbeta and SPbetaL8, and intermediate, weaker defense against phages SPbetaL6 and SPbetaL7 (fig. 1c, ED fig. 2a). The remaining seven phages of the SPbeta group were able to completely overcome Gabija-mediated defense. We found two genes that were present in the seven Gabija-overcoming phages while missing from phages that were sensitive to Gabija defense (fig. 2a, ED fig. 1a, Supplementary table 7). One of these genes (ORF 129; Supplementary table 7) did not show a Gabija-inhibiting phenotype when co-expressed with Gabija, and we were unable to clone the second gene (ORF128) into Gabija-expressing cells, presumably due to toxicity. To examine the possible function of the non-cloned ORF128 gene, we knocked out that gene from the genome of phage phi3T. Our results show that phi3T knocked out for ORF128 was no longer able to overcome Gabija defense, suggesting that this gene inhibits Gabija (fig. 2b). We denote the anti-Gabija gene *gad1* (Gabija anti-defense 1). Engineering *gad1* from phi3T together with its native promoter into the genome of phage SPbeta, which naturally lacks this gene, rendered SPbeta resistant to Gabija, confirming that *gad1* is both necessary and sufficient for the anti-Gabija phenotype (fig. 2b).

Gad1 is a 295 aa-long protein, which does not exhibit sequence similarity to proteins of known function. We found 94 homologs of Gad1, distributed in genomes of various phages and prophages infecting host bacteria from the phyla *Proteobacteria* and *Firmicutes* (fig. 2c, Supplementary tables 8,9). Interestingly, many of the Gad1-containing prophages were integrated in bacterial genomes that also encoded the Gabija system, suggesting that Gad1 enabled these phages to overcome Gabija-mediated defense of their hosts (fig. 2c). Five Gad1 homologs from phages infecting *Shewanella sp.*, *Enterobacter roggenkampii*, *Escherichia coli*, *Brevibacillus gelatini* and *Bacillus xiamenensis* were selected for further experimental examination as representatives of the phylogenetic diversity of the Gad1 family (fig. 2c, ED fig. 3a). Unlike the Gad1 protein from phage phi3T, four of the Gad1 homologs were not toxic when expressed in Gabija-containing cells (all except the homolog cloned from the *B. xiamenensis* prophage). Each of these four homologs efficiently inhibited Gabija defense when co-expressed in Gabija-containing cells (fig. 2d, ED fig. 3b).

It was recently shown that Gabija identifies and cleaves DNA having a specific nearly palindromic sequence motif derived from phage Lambda[40]. By purifying GajA and GajB and reconstituting the Gabija complex *in vitro*, we were able to confirm that Gabija cleaves DNA that contains the specific sequence motif (fig. 2e). Gabija purified in the presence of Gad1 was unable to cleave DNA (fig. 2e). In a companion paper, we show that Gad1 binds the Gabija complex as an octamer and inhibits its ability to bind and cleave DNA[42].

We next examined phages SPbetaL6 and SPbetaL7, which lack *gad1* but were still partially resistant to Gabija (fig. 1c). Intriguingly, these phages encoded, at the same locus where *gad1* was encoded in other phages, another gene of unknown function. Knocking-out this gene from phage SPbetaL7 rendered this phage completely sensitive to Gabija (fig. 2f). The gene from SPbetaL7 was toxic when expressed in bacteria, but co-expression of a non-toxic homolog from a prophage of *Brevibacillus laterosporus* with Gabija completely inhibited Gabija defense, further verifying that it is an anti-Gabija gene which we denote here *gad2* (fig. 2a,f). Gad2 is a 400 aa-long protein that shows no sequence similarity to Gad1 or to other known proteins. Homology searches identified 170 homologs of Gad2 which almost always reside in genomes of phages and prophages infecting diverse host bacteria (ED fig. 4a, Supplementary tables 10,11). Intriguingly, structural analysis using Alphafold2[43] predicted that Gad2 is an enzyme with a nucleotidyltransferase protein domain, suggesting that it inhibits Gabija via a mechanism of action

136 different than Gad1 (ED fig. 4b). Point mutations in residues predicted to form the active site of the *B.*
137 *laterosporus* Gad2 nucleotidyltransferase domain rendered Gad2 inactive, suggesting that a
138 nucleotidyltransferase activity is necessary for the anti-defense function (ED fig. 4c). Purified *B.*
139 *laterosporus* Gad2 did not bind the Gabija complex *in vitro* and did not inhibit DNA cleavage, implying
140 that Gad2 may operate upstream to Gabija to modify the phage molecules sensed by the GajA–GajB
141 defense complex (ED fig. 4d-f). Combined together, our results suggest that SPbeta-like phages encode
142 anti-Gabija genes in a dedicated locus in their genomes, where multiple different Gabija-inhibiting genes
143 can reside.
144
145 Phage genes that inhibit Thoeris
146
147 The Thoeris defense system is present in approximately 4% of sequenced bacterial and archaeal
148 genomes[18]. This system encodes ThsB, a protein with a Toll/interleukin-1 receptor (TIR) domain that
149 serves as a sensor for phage infection, and ThsA, an NAD^+-cleaving protein[27]. Upon phage recognition,
150 the Thoeris ThsB protein generates 1″–3′ gcADPR, a signaling molecule that activates ThsA, resulting in
151 the depletion of NAD^+ and the inhibition of phage replication[33].
152
153 Our recent discovery of the anti-Thoeris gene *tad1*, a 1″–3′ gcADPR sponge present in phage SBSphiJ7
154 and absent from other phages in the SBSphiJ group, explains the observed insensitivity of SBSphiJ7 to
155 Thoeris[33] (fig. 1c, ED fig. 2c). We hypothesized that phages SPO1 and SPO1L3 may also encode
156 homologs of *tad1*, as these phages partially escaped Thoeris-mediated defense (fig. 1c, ED fig. 2b), but
157 we were unable to identify *tad1* homologs in these phages. Instead, we identified a single gene present in
158 SPO1 and SPO1L3 but absent from all other Thoeris-sensitive SPO1-like phages (fig. 3a, Supplementary
159 table 7). We expressed this gene, designated here *tad2,* within *B. subtilis* cells that also express the Thoeris
160 system from *B. cereus* MSX-D12. Tad2 robustly inhibited the activity of Thoeris, allowing Thoeris-
161 sensitive phages to infect Thoeris-expressing cells (fig. 3b). Moreover, engineering *tad2* into SBSphiJ, a
162 phage that is normally blocked by Thoeris, resulted in a phage that overcomes Thoeris-mediated defense
163 (fig. 3b). Silencing the expression of Tad2 in SPO1 using dCas9[44] further confirmed that Tad2 is
164 responsible for the Thoeris-inhibiting phenotype of SPO1 (fig. 3c).
165
166 Tad2 is a short protein (89 aa) containing a DUF2829 protein domain. Sequence homology searches
167 identified over 650 homologs in the integrated microbial genomes (IMG)[45] and metagenomic gut virus
168 (MGV)[46] databases (Supplementary tables 12,13). Phylogenetic analysis revealed that Tad2 is encoded by
169 phages belonging to several phage morphology groups, including *Myoviridae*, *Podoviridae* and
170 *Siphoviridae*, as well as by prophages integrated within over 100 bacterial species from 6 different phyla
171 (fig. 3d). We selected 5 Tad2 homologs representing the phylogenetic diversity of the family and cloned
172 each one separately into *B. subtilis* cells expressing the Thoeris system (fig. 3d, ED fig. 5a). Four of these
173 Tad2 homologs were able to inhibit Thoeris, including homologs derived from phages infecting distant
174 organisms such as *Ruminococcus callidus* and *Maridesulfovibrio bastinii* (ED fig. 5b). These results
175 demonstrate that Tad2 represents a large family of proteins used by phages to inhibit the Thoeris defense
176 system.
177
178 During phage infection, ThsB generates the 1″–3′ gcADPR signaling molecule to activate ThsA[33]. As
179 expected, purified ThsA incubated with filtered cell lysates derived from SBSphiJ-infected, ThsB-
180 expressing cells became a strong NADase, indicating that ThsB produced 1″–3′ gcADPR in response to
181 SBSphiJ infection as previously shown[33] (fig. 4a). However, filtered lysates from similarly infected cells

182 that co-expressed both ThsB and Tad2 failed to activate ThsA *in vitro*, suggesting that Tad2 functions
183 upstream of ThsA (fig. 4a).
184
185 Recent studies have shown that phages can use dedicated proteins to degrade[32,47] or sequester[31,33] bacterial
186 immune signaling molecules. Incubation of Tad2 with 1″–3′ gcADPR *in vitro* did not yield observable
187 degradation products, suggesting that Tad2 is not an enzyme that cleaves 1″–3′ gcADPR (ED fig. 6a). To
188 test whether Tad2 might act as a sponge that binds and sequesters the immune signal, we incubated
189 purified Tad2 with 1″–3′ gcADPR, and then heated the reaction at 95 °C to denature Tad2. The denatured
190 reaction readily activated ThsA, suggesting that Tad2 functions by binding and sequestering the Thoeris-
191 derived signaling molecule, and that denaturation of Tad2 released the intact molecule back to the medium
192 (fig. 4b). In support of this observation, Tad2 that was pre-incubated with 1″–3′ gcADPR showed a
193 substantial mobility shift during size-exclusion chromatography (ED fig. 6b). In addition, Tad2 exhibited
194 increased absorption ratio of UV_{260nm}/UV_{280nm} following incubation with 1″–3′ gcADPR, further
195 confirming that Tad2 binds this molecule as a ligand (ED fig. 6b). We found that Tad2 binds 1″–3′
196 gcADPR with K_d = 23.3 nM (ED fig. 6c). Notably, Tad2 could not bind the canonical cADPR,
197 demonstrating high specificity of Tad2 to the ThsB-derived signaling molecule (ED fig. 6d).
198
199 To define the mechanism of 1″–3′ gcADPR sequestration and Thoeris inhibition, we determined crystal
200 structures of Tad2 from phage SPO1 in the apo and 1″–3′ gcADPR ligand-bound states (ED Table 1). We
201 also determined crystal structures of Tad2 bound to 1″–2′ gcADPR and Tad1 from phage *Clostridium*
202 *botulinum* bound to 1″–3′ gcADPR (ED table 1). The structures of Tad2 reveal a homotetrameric assembly
203 consistent with oligomerization observed during size-exclusion chromatography analysis (ED fig. 7). Two
204 Tad2 protomers pack together at helix α2 and sheet β2 to form V-shaped homodimeric units, which then
205 interlock perpendicularly along helix α1 to complete tetramerization (fig. 4c, ED fig. 8). The resulting
206 assembly creates two identical ligand binding pockets formed at the interface of two adjacent non-dimeric
207 protomers, surrounded by loop β1–β2, loop β3–β4, and strand β4 of one protomer, and loop β1–β2, loop
208 β4–α3, and helix α3 of the other (fig. 4c–f).
209
210 A 1.75 Å structure of Tad2 in complex with 1″–3′ gcADPR explains the molecular basis of signal
211 recognition. In the Tad2–1″–3′ gcADPR complex, ligand binding is mediated by extensive van der Waals
212 interactions from $W25_{a,b}$ and $W73_{a,b}$, as well as polar interactions to phosphates and free hydroxyls from
213 $N26_{a,b}$ and $D79_{a,b}$ (fig. 4e,f). Compared to the Tad1–1″–3′ gcADPR complex, Tad2 forms very few
214 contacts to the adenine base of 1″–3′ gcADPR, with one hydrogen bond from $T78_b$ and nonpolar
215 interactions from $I63_a$ and $T65_a$, while Tad1 forms base stacking interactions via $F82_b$ and $R109_a$, as well
216 as specific hydrogen bonding to the Hoogsteen edge via $N92_b$ (fig 4e,f, ED fig. 8). Additionally, we
217 observed several key water molecules in the Tad2 structure that contribute to 1″–3′ gcADPR binding and
218 are coordinated by $N26_b$, $D67_a$, $H71_a$, $W73_b$, $S76_b$, and $D79_{a,b}$ (fig. 4e,f). Tad2 binds both 1″–3′ gcADPR
219 and 1″–2′ gcADPR via the same binding residues, and both molecules are oriented nearly identically in
220 the Tad2 binding pocket (ED fig. 8b,c). Although the molecular basis for ligand recognition is dissimilar
221 between Tad2 and Tad1, we observe that Tad1, too, binds both 1″–3′ gcADPR and 1″–2′ gcADPR in the
222 same pocket and orientation (ED fig. 8e,f), highlighting how both proteins function as sponges for
223 gcADPR molecules. Taken together, our findings show that Tad2 inhibits Thoeris defense by binding and
224 sequestering 1″–3′ gcADPR, preventing the activation of the Thoeris immune effector and mitigating
225 Thoeris-mediated defense.
226
227 <u>Phage genes that inhibit Hachiman</u>

Hachiman is a defense system whose mechanism of action remains unsolved. It encodes a protein with a predicted helicase domain, as well as an additional protein with no known functional domains. Hachiman is found in over 3% of sequenced bacterial and archaeal genomes, and was shown to provide strong protection against a broad range of phages[18].

We cloned three short genes that were unique to phage SBSphiJ4, a phage that overcame Hachiman-mediated defense (fig. 1c, Supplementary table 7), into a *B. subtilis* strain that expresses the Hachiman system from *B. cereus* B4087 [18]. One of these genes completely abolished Hachiman-mediated defense, and we therefore named it *had1* (Hachiman anti-defense 1) (fig. 5a,b). Silencing of Had1 expression in SBSphiJ4 resulted in a phage that could infect control strains, but was blocked by Hachiman defense (fig. 5c). In addition, SBSphiJ that was engineered to include Had1 with its native promoter was able to overcome Hachiman defense, demonstrating that Had1 is responsible for the anti-Hachiman phenotype (fig. 5b).

Had1 is a short protein sized 53 aa, which does not show sequence homology to any protein of known function. We found 23 homologs of Had1 in *Bacillus* phages as well as prophages integrated within *Bacillus* and *Paenibacillus* genomes (Supplementary table 14), and selected five homologs that span the protein sequence diversity of Had1 for further experimental examination. Four of these proteins efficiently inhibited the activity of Hachiman, and we could not clone the fifth into Hachiman-expressing cells, possibly due to toxicity (ED fig. 9a,b). These results confirm that Had1 is a Hachiman-inhibiting family of phage proteins.

We determined the crystal structure of Had1 from *Bacillus toyonensis*, revealing a homodimeric complex with two splayed loops that form an overall platform-like shape (fig. 5d, ED fig. 9c,d). The Had1 dimeric interface consists of four beta strands, two contributed by each protomer (fig 5d). At the center of the Had1 complex platform there is a positively charged patch formed by conserved residues in strand β2 including R17 and K18 (fig. 5e). A Had1 residue I41 at the center of the dimeric interface in each protomer forms hydrophobic packing interactions with five residues on the other protomer, supporting the dimerization interface (fig. 5f). Mutation of the equivalent isoleucine residue in SBSphiJ4 Had1 rendered the protein unable to inhibit Hachiman, suggesting that the dimeric structure is necessary for Had1 evasion of host anti-phage defense (fig 5g).

It was previously shown that the SBSphiJ phage can escape Hachiman defense by mutating its ssDNA-binding (SSB) protein, and it was hypothesized that Hachiman may recognize protein-DNA complexes produced as an intermediate of phage DNA replication or recombination[41]. The positively charged patch at the center of the Had1 dimeric complex (fig. 5e) may imply that Had1 might shield phage replication intermediates from being recognized by the Hachiman system. As the mechanism of Hachiman defense is currently unknown, understanding how Had1 inhibits Hachiman in future studies may assist in solving the mechanism of Hachiman defense.

In this study we identified multiple families of phage anti-defense proteins using comparative analysis of closely-related phage genomes. Our findings demonstrate that phages have evolved diverse strategies to counter the complex, multilayered bacterial defense arsenal. Intriguingly, our data suggest that SPbeta-like phages store anti-Gabija genes in a dedicated anti-Gabija locus in their genomes. This is reminiscent of anti-CRISPR loci identified in phages of *Pseudomonas* and other species, where different sets of anti-CRISPR genes are present in each individual phage[48]. Our discovery of a specific anti-Gabija locus in SPbeta-like phages may point to a general rule for the organization of anti-defense genes in phage genomes, a genomic phenomenon that can assist in future searches for anti-defense genes.

The most widely distributed family of anti-defense proteins discovered here is that of Tad2, a protein that contains a domain of unknown function DUF2829. A protein with DUF2829 was previously speculated to inhibit type II CRISPR-Cas systems and specifically Cas9 [49], although binding to Cas9 was not demonstrated and the mechanism through which this protein antagonizes type II CRISPR-Cas was not determined[49]. Our findings that multiple DUF2829-containing proteins antagonize the Thoeris defense system by specifically binding and sequestering 1″–3′ gcADPR suggest that the DUF2829 family of proteins represent anti-Thoeris proteins rather than anti-CRISPR proteins.

Our results on Tad2 join recent discoveries of additional anti-defense proteins that function by sequestering immune signaling molecules[31,33]. These include Tad1, a completely different family of Thoeris-inhibiting proteins, which, similar to Tad2, also bind and sequester gcADPR molecules; and the phage-encoded Acb2 protein that inhibits CBASS defense by binding the cyclic oligonucleotide immune signaling molecules produced by CBASS[31,33]. It therefore appears that the production of protein "sponges" that sequester immune signaling molecules is a highly efficient strategy that evolved within phages multiple times in parallel to allow successful evasion of immune systems that utilize immune signaling molecules. The efficiency of this strategy may be perceived as counter-intuitive, because it necessitates a 1:1 ratio between the number of phage sponge proteins and the immune signaling molecule (or even 2:1 in the case of Tad2). However, as Thoeris and CBASS become active and produce the immune signaling molecule relatively late in the infection cycle of the phage[20,27], phages have sufficient time to express a substantial amount of their sponge proteins at the early stages of infection. Thus, when the immune signaling molecule is produced by the defense system, there will already be enough copies of the sponge protein in the infected cell to efficiently block immune signaling. An alternative explanation for the efficiency of phage sponges could be that they have a higher affinity to the signaling molecule as compared to the bacterial effector. The affinity we measured for Tad2 binding to 1″–3′ gcADPR (K_d = 23.3 nM; ED fig. 6c), is indeed higher than the affinity measured for binding of the same molecule to Thoeris ThsA (K_d = 59.1 nM[50]), but both are within the same order of magnitude of nanomolar affinity.

We were not able to identify inhibitors of the Septu or Lamassu defense systems among the three groups of phages that we studied, although phages from these groups displayed differential sensitivity to these defense systems. It is possible that escape from these two systems is mediated by mutations in existing genes rather than the presence of a dedicated anti-defense gene[41]. It is also possible that different phages in the same group utilize more than one protein to overcome defense, which would sometime hamper the analysis pipeline used in this study.

With the emergence of multiple antibiotic-resistant bacteria[51], phage therapy, in which phages are used as an alternative to antibiotics, is being considered as a suitable therapeutic avenue for defeating bacterial pathogens[52–54]. One of the major obstacles for successful phage therapy is the recently discovered ability

of bacteria to actively defend themselves by encoding a large variety of defense systems. Indeed, it was shown that the set of defense systems carried by a given bacterial strain is a strong determinant for the susceptibility of that strain to phages[55,56]. Engineering phages to carry a set of anti-defense proteins can enable them to overcome bacterial defenses, resulting in phages with increased host ranges that will be more suitable for phage therapy. Thus, the anti-defense proteins we discovered here, as well as additional such proteins that were discovered and will be discovered in the future, could be used as tools for more efficient phage therapy applications.

References

1. Dy, R. L., Richter, C., Salmond, G. P. C. & Fineran, P. C. Remarkable mechanisms in microbes to resist phage infections. *Annu. Rev. Virol.* **1**, 307–331 (2014).
2. Bernheim, A. & Sorek, R. The pan-immune system of bacteria: antiviral defence as a community resource. *Nat. Rev. Microbiol.* **18**, 113–119 (2020).
3. Hampton, H. G., Watson, B. N. J. & Fineran, P. C. The arms race between bacteria and their phage foes. *Nature* **577**, 327–336 (2020).
4. Tal, N. & Sorek, R. SnapShot: Bacterial immunity. *Cell* **185**, 578-578.e1 (2022).
5. Samson, J. E., Magadán, A. H., Sabri, M. & Moineau, S. Revenge of the phages: defeating bacterial defences. *Nat. Rev. Microbiol.* **11**, 675–687 (2013).
6. C. Atanasiu, T.-J. Su, S. S. Sturrock, D. T. F. D. Interaction of the ocr gene 0.3 protein of bacteriophage T7 with EcoKI restriction/modification enzyme. *Nucleic Acids Res.* **30**, 3936–3944 (2002).
7. Walkinshaw, M. . *et al.* Structure of Ocr from bacteriophage T7, a protein that mimics B-form DNA. *Mol. Cell* **9**, 187–194 (2002).
8. Drozdz, M., Piekarowicz, A., Bujnicki, J. M. & Radlinska, M. Novel non-specific DNA adenine methyltransferases. *Nucleic Acids Res.* **40**, 2119–2130 (2012).
9. Thavalingam, A. *et al.* Inhibition of CRISPR-Cas9 ribonucleoprotein complex assembly by anti-CRISPR AcrIIC2. *Nat. Commun.* **10**, 2806 (2019).
10. Lu, W.-T., Trost, C. N., Müller-Esparza, H., Randau, L. & Davidson, A. R. Anti-CRISPR AcrIF9 functions by inducing the CRISPR–Cas complex to bind DNA non-specifically. *Nucleic Acids Res.* **49**, 3381–3393 (2021).
11. Bondy-Denomy, J. *et al.* Multiple mechanisms for CRISPR–Cas inhibition by anti-CRISPR proteins. *Nature* **526**, 136–139 (2015).
12. Stanley, S. Y. & Maxwell, K. L. Phage-Encoded Anti-CRISPR Defenses. *Annu. Rev. Genet.* **52**, 445–464 (2018).
13. Li, Y. & Bondy-Denomy, J. Anti-CRISPRs go viral: The infection biology of CRISPR-Cas inhibitors. *Cell Host Microbe* **29**, 704–714 (2021).
14. Jia, N. & Patel, D. J. Structure-based functional mechanisms and biotechnology applications of anti-CRISPR proteins. *Nat. Rev. Mol. Cell Biol.* **22**, 563–579 (2021).
15. Davidson, A. R. *et al.* Anti-CRISPRs: Protein Inhibitors of CRISPR-Cas Systems. *Annu. Rev. Biochem.* **89**, 309–332 (2020).
16. Otsuka, Y. & Yonesaki, T. Dmd of bacteriophage T4 functions as an antitoxin against Escherichia coli LsoA and RnlA toxins. *Mol. Microbiol.* **83**, 669–681 (2012).
17. Blower, T. R., Evans, T. J., Przybilski, R., Fineran, P. C. & Salmond, G. P. C. Viral evasion of a bacterial suicide system by RNA–based molecular mimicry enables infectious altruism. *PLoS Genet.* **8**, e1003023 (2012).

18. Doron, S. *et al.* Systematic discovery of antiphage defense systems in the microbial pangenome. *Science* **359**, eaar4120 (2018).
19. Gao, L. *et al.* Diverse enzymatic activities mediate antiviral immunity in prokaryotes. *Science* **369**, 1077–1084 (2020).
20. Cohen, D. *et al.* Cyclic GMP–AMP signalling protects bacteria against viral infection. *Nature* **574**, 691–695 (2019).
21. Millman, A. *et al.* Bacterial retrons function in anti-phage defense. *Cell* **183**, 1551-1561.e12 (2020).
22. Bernheim, A. *et al.* Prokaryotic viperins produce diverse antiviral molecules. *Nature* **589**, 120–124 (2021).
23. Millman, A. *et al.* An expanded arsenal of immune systems that protect bacteria from phages. *Cell Host Microbe* **30**, 1556-1569.e5 (2022).
24. Whiteley, A. T. *et al.* Bacterial cGAS-like enzymes synthesize diverse nucleotide signals. *Nature* **567**, 194–199 (2019).
25. Lau, R. K. *et al.* Structure and mechanism of a cyclic trinucleotide-activated bacterial endonuclease mediating bacteriophage immunity. *Mol. Cell* **77**, 723-733.e6 (2020).
26. Millman, A., Melamed, S., Amitai, G. & Sorek, R. Diversity and classification of cyclic-oligonucleotide-based anti-phage signalling systems. *Nat. Microbiol.* **5**, 1608–1615 (2020).
27. Ofir, G. *et al.* Antiviral activity of bacterial TIR domains via immune signalling molecules. *Nature* **600**, 116–120 (2021).
28. Tal, N. *et al.* Cyclic CMP and cyclic UMP mediate bacterial immunity against phages. *Cell* **184**, 5728-5739.e16 (2021).
29. Kronheim, S. *et al.* A chemical defence against phage infection. *Nature* **564**, 283–286 (2018).
30. Bobonis, J. *et al.* Bacterial retrons encode phage-defending tripartite toxin–antitoxin systems. *Nature* **609**, 144–150 (2022).
31. Huiting, E. *et al.* Bacteriophages inhibit and evade cGAS-like immune function in bacteria. *Cell* **186**, 864-876.e21 (2023).
32. Hobbs, S. J. *et al.* Phage anti-CBASS and anti-Pycsar nucleases subvert bacterial immunity. *Nature* **605**, 522–526 (2022).
33. Leavitt, A. *et al.* Viruses inhibit TIR gcADPR signalling to overcome bacterial defence. *Nature* **611**, 326–331 (2022).
34. Rosenthal, R., Toye, P. A., Korman, R. Z. & Zahler, S. A. The prophage of SP beta c2dcitK1, A defective specialized transducing phage of Bacillus subtilis. *Genetics* **92**, 721–739 (1979).
35. Tucker, R. G. Acquisition of thymidylate synthetase activity by a thymine-requiring mutant of Bacillus subtilis following Infection by the temperate phage φ3. *J. Gen. Virol.* **4**, 489–504 (1969).
36. Noyer-Weidner, M., Jentsch, S., Pawlek, B., Günthert, U. & Trautner, T. A. Restriction and modification in Bacillus subtilis: DNA methylation potential of the related bacteriophages Z, SPR, SP beta, phi 3T, and rho 11. *J. Virol.* **46**, 446–453 (1983).
37. Stewart, C. R. *et al.* The Genome of Bacillus subtilis Bacteriophage SPO1. *J. Mol. Biol.* **388**, 48–70 (2009).
38. Gilchrist, C. L. M. & Chooi, Y.-H. clinker & clustermap.js: automatic generation of gene cluster comparison figures. *Bioinformatics* **37**, 2473–2475 (2021).
39. Tesson, F. *et al.* Systematic and quantitative view of the antiviral arsenal of prokaryotes. *Nat. Commun.* **13**, 2561 (2022).
40. Cheng, R. *et al.* A nucleotide-sensing endonuclease from the Gabija bacterial defense system. *Nucleic Acids Res.* **49**, 5216–5229 (2021).

41. Stokar-Avihail, A. *et al.* Discovery of phage determinants that confer sensitivity to bacterial immune systems. *Cell* **186**, 1863-1876.e16 (2023).
42. Antine, S. P. *et al.* Structural basis of Gabija anti-phage defense and viral immune evasion. *bioRxiv* 2023.05.01.538945 (2023) doi:10.1101/2023.05.01.538945.
43. Jumper, J. *et al.* Highly accurate protein structure prediction with AlphaFold. *Nature* **596**, 583–589 (2021).
44. Peters, J. M. *et al.* A comprehensive, CRISPR-based functional analysis of essential genes in bacteria. *Cell* **165**, 1493–1506 (2016).
45. Chen, I.-M. A. *et al.* IMG/M v.5.0: an integrated data management and comparative analysis system for microbial genomes and microbiomes. *Nucleic Acids Res.* **47**, D666–D677 (2019).
46. Nayfach, S. *et al.* Metagenomic compendium of 189,680 DNA viruses from the human gut microbiome. *Nat. Microbiol.* **6**, 960–970 (2021).
47. Athukoralage, J. S. *et al.* An anti-CRISPR viral ring nuclease subverts type III CRISPR immunity. *Nature* **577**, 572–575 (2020).
48. Bondy-Denomy, J., Pawluk, A., Maxwell, K. L. & Davidson, A. R. Bacteriophage genes that inactivate the CRISPR/Cas bacterial immune system. *Nature* **493**, 429–432 (2013).
49. Uribe, R. V. *et al.* Discovery and Characterization of Cas9 Inhibitors Disseminated across Seven Bacterial Phyla. *Cell Host Microbe* **25**, 233-241.e5 (2019).
50. Manik, M. K. *et al.* Cyclic ADP ribose isomers: Production, chemical structures, and immune signaling. *Science* **377**, eadc8969 (2022).
51. MacLean, R. C. & San Millan, A. The evolution of antibiotic resistance. *Science* **365**, 1082–1083 (2019).
52. Kortright, K. E., Chan, B. K., Koff, J. L. & Turner, P. E. Phage therapy: A renewed approach to combat antibiotic-resistant bacteria. *Cell Host Microbe* **25**, 219–232 (2019).
53. Nobrega, F. L., Costa, A. R., Kluskens, L. D. & Azeredo, J. Revisiting phage therapy: new applications for old resources. *Trends Microbiol.* **23**, 185–191 (2015).
54. Federici, S. *et al.* Targeted suppression of human IBD-associated gut microbiota commensals by phage consortia for treatment of intestinal inflammation. *Cell* **185**, 2879-2898.e24 (2022).
55. Hussain, F. A. *et al.* Rapid evolutionary turnover of mobile genetic elements drives bacterial resistance to phages. *Science* **374**, 488–492 (2021).
56. LeGault, K. N. *et al.* Temporal shifts in antibiotic resistance elements govern phage-pathogen conflicts. *Science* **373**, (2021).

Figure Legends

Figure 1. Identification of anti-defense genes based on differential sensitivity to defense systems. (a) A flowchart of the experiments and analyses used in this study to detect candidate anti-defense genes. (b) Genome comparison of six phages from the SPO1 group. Amino acid sequence similarity is marked by grey shading. Genome similarity was visualized using clinker[38]. (c) Infection profile of SBSphiJ-like, SPbeta-like and SPO1-like phages infecting five *Bacillus subtilis* strains that express each of the defense systems Thoeris, Hachiman, Gabija, Septu and Lamassu. Fold defense was measured using serial dilution plaque assays, comparing the efficiency of plating (EOP) of phages on the system-containing strain to the EOP on a control strain that lacks the systems and contains an empty vector instead. Data represent an average of three replicates. Detailed data from individual plaque assays are found in ED fig. 2.

Figure 2. Gad1 and Gad2 proteins inhibit Gabija defense. (a) The anti-Gabija locus in phages of the SPbeta group. Amino acid sequence similarity is marked by grey shading. Genome similarity was visualized using Clinker[38]. (b) Deletion of *gad1* from phage phi3T eliminates the ability of the phage to cancel Gabija-mediated defense, while knock in of *gad1* into phage SPbeta renders the phage resistant to Gabija. Data represent plaque-forming units per ml (PFU/ml) of phages infecting control cells ("no system") and cells expressing the Gabija defense system. Shown is the average of three technical replicates, with individual data points overlaid. (c) Phylogeny and distribution of Gad1 homologs. The names of bacteria in which Gad1 homologs were found in prophages and verified experimentally are indicated on the tree by cyan diamonds. (d) Results of phage infection experiments. Data represent plaque-forming units per ml (PFU/ml) of SPbeta infecting control cells ("no system"), cells expressing the Gabija system ("Gabija"), and cells co-expressing the Gabija system and a Gad1 homolog. Shown is the average of three technical replicates, with individual data points overlaid. (e) Gad1 blocks Gabija-mediated DNA cleavage. Incubation of purified Gabija (GajAB) complex, or Gabija co-purified with Gad1 from *Shewanella sp.* phage 1/4 (GajAB + Gad1) with a previously described DNA substrate from phage Lambda[40]. Shown is representative agarose gel from three independent experiments of proteins with 1, 5, 10, 15 or 20 min incubation with DNA. (f) Knockout of *gad2* from phage SPbetaL7 renders the phage sensitive to Gabija defense, while expression of a Gad2 homolog from a *Brevibacillus laterosporus* prophage allows SPbeta to overcome Gabija-mediated defense. Phage infection experiments were conducted as in panel (d).

Figure 3. Tad2 proteins inhibit Thoeris defense. (a) Genomic locus of the anti-Thoeris gene *tad2* in phages SPO1 and SPO1L3, and the respective locus in phages SPO1L4 and SPO1L2. Amino acid sequence similarity is marked by grey shading. Genome similarity was visualized using Clinker[38]. (b) Anti-Thoeris activity of Tad2. Data represent plaque-forming units per milliliter (PFU/ml) of phages infecting control cells (no system), cells expressing the Thoeris system (Thoeris) and cells co-expressing the Thoeris system and the *tad2* gene from SPO1 (Thoeris + Tad2). Data for phage SBSphiJ as well as for SBSphiJ with a *tad2* knock in are also presented. Shown is the average of three technical replicates, with individual data points overlaid. (c) Tad2 knockdown cancels anti-Thoeris activity. Data represent PFU/ml of SPO1 that infects cells expressing Thoeris and a dCas9 system targeting Tad2, as well as control cells. Shown is the average of three technical replicates, with individual data points overlaid. (d) Phylogenetic analysis of Tad2 homologs in phage and prophage genomes. The names of bacteria in which Tad2 homologs were found in prophages and tested experimentally are indicated on the tree by cyan diamonds.

Figure 4. Tad2 cancels Thoeris-mediated defense by sequestering 1″–3′ gcADPR. (a) Cells expressing ThsB, both ThsB and Tad2 or control cells that do not express ThsB were infected with phage SBSphiJ at a multiplicity of infection (MOI) of 10. NADase activity of purified ThsA incubated with filtered lysates was measured using a nicotinamide 1,N6-ethenoadenine dinucleotide (εNAD) cleavage fluorescence assay. Bars represent the mean of three experiments, with individual data points overlaid. (b) Tad2 releases bound 1″–3′ gcADPR when denatured. Shown is the NADase activity of purified ThsA incubated with 600nM 1″–3′ gcADPR preincubated with 2.4 μM of purified Tad2 *in vitro* for 10 min, followed by an additional incubation of 10 min at either 25 °C or 95 °C. Control is buffer without 1″–3′ gcADPR. Bars represent the mean of three experiments, with individual data points overlaid. (c) Overview of the crystal structure of Tad2 in complex with 1″–3′ gcADPR in cartoon (front) or surface (side) representation. Tad2 exists as a homotetramer formed by two dimer units (colored cyan/dark blue and grey/dark grey). Non-dimeric monomer pairs form two recessed ligand binding pockets that enclose 1″–3′ gcADPR. (d) Topology map of two Tad2 monomers which come together to form the ligand binding pocket.

502 Components that form the binding pocket are outlined in green. Each dimer subunit donates one monomer,
503 as shown by the cartoon representation. (e,f) Detailed views centered around the adenine base (e) or ribose
504 and phosphates (f) of residues that either directly interact with 1″–3′ gcADPR or coordinate key waters
505 that reside within the binding pocket. Residues contributed by each of the two monomers that form the
506 binding pocket are represented in cyan ($Tad2_a$) or grey ($Tad2_b$) .

507 **Figure 5. Had1 proteins inhibit Hachiman defense.** (a) Genomic locus of the anti-Hachiman gene *had1*
508 in phages SBSphiJ4, as well as the relevant locus in phage SBSphiJ7, SBSphiJ and SBSphiJ5. Amino acid
509 sequence similarity is marked by grey shading. Genome similarity was visualized using clinker[38]. (b)
510 Differential defense of Hachiman against phages from the SBSphiJ group, and anti-Hachiman activity of
511 Had1. Data represent plaque-forming units per milliliter (PFU/ml) of phages infecting control cells (no
512 system), cells expressing the Hachiman system (Hachiman) and cells co-expressing the Hachiman system
513 and the *had1* gene from SBSphiJ4 (Hachiman + Had1). Data for phage SBSphiJ with a *had1* knock-in are
514 also presented. Shown is the average of three technical replicates, with individual data points overlaid. (c)
515 Had1 knockdown cancels anti-Hachiman activity. Results of phage SBSphiJ4 infection experiments. Data
516 represent plaque-forming units per ml (PFU/ml) of SBSphiJ4 infecting cells expressing Hachiman and a
517 dCas9 with an sgRNA targeting Had1, as well as control cells. Shown is the average of three technical
518 replicates, with individual data points overlaid. (d,e) *Bacillus toyonensis* Had1 structure overview and
519 surface electrostatics. Had1 is a homodimer (colored red/light grey) with a central β-barrel core formed
520 by strands β1–β3 and splayed loops that create a complex with an overall platform-like shape. (f) Zoomed
521 in cutaway and sequence alignment of *B. toyonensis* Had1 residue I41 that forms hydrophobic packing
522 interactions with T11, I16, Y35, A37, and A39 from the opposing protomer. (g) Had1 mutations at the
523 center of the dimeric interface result in loss of anti-defense activity. Data represent plaque-forming units
524 per ml (PFU/ml) of phage SBSphiJ infecting cells that co-express the Hachiman system and WT or
525 mutated Had1 from phage SBSphiJ4, as well as control cells lacking Had1 and control cells lacking both
526 Had1 and Hachiman. Shown is the average of three technical replicates, with individual data points
527 overlaid.
528
529 **Methods**
530
531 Bacterial strains and growth conditions
532
533 Bacteria were grown in magnesium manganese broth (MMB) (LB + 0.1 mM $MnCl_2$ + 5 mM $MgCl_2$) at
534 37 °C shaking at 200 rpm, unless specified otherwise. To ensure the presence of an integrated antibiotics
535 resistance cassette in the *B. subtilis* genome, the appropriate antibiotics were added at the following
536 concentration: spectinomycin (100 μg ml^{-1}) or chloramphenicol (5 μg ml^{-1}). *Escherichia coli* strain *E.*
537 *coli* NEB 5-alpha (NEB cat #C2987H) was grown in LB. Whenever applicable, media were supplemented
538 with ampicillin (100 μg/ml).
539
540 Defense systems used in this study were cloned previously by Doron et. al.[18] under their native promoter
541 into the *amyE* locus of the *B. subtilis* BEST7003 genome. The source organisms of the specific systems
542 used in this study are as follows: Thoeris (*Bacillus cereus* MSX-D12), Hachiman (*B. cereus* B4087),
543 Gabija (*B. cereus* VD045), Septu (*Bacillus thuringiensis* HD12), and Lamassu (*Bacillus sp.* NIO-1130).
544
545
546 Phage strains, isolation, cultivation and sequencing

547
548 *B. subtilis* phages phi3T (BGSCID 1L1, GenBank accession KY030782.1), SPbeta (BGSCID 1L5,
549 GenBank accession AF020713.1), SPR (BGSCID 1L56, GenBank accession OM236515.1) and SPO1
550 (BGSCID 1P4, GenBank accession NC_011421.1) were obtained from the Bacillus Genetic Stock Center
551 (BGSC). Phages from the SBSphiJ group were isolated by us in previous studies[18,33]. Other phages used
552 in this study were isolated by us from soil samples on *B. subtilis* BEST7003 culture as described in Doron
553 *et al.*[18]. For this, soil samples were added to *B. subtilis* BEST7003 culture and incubated overnight to
554 enrich for *B. subtilis* phages. The enriched sample was centrifuged and filtered through 0.45 µm filters,
555 and the filtered supernatant was used to perform double layer plaque assays as described in Kropinski *et*
556 *al.*[57]. Single plaques that appeared after overnight incubation at RT were picked, re-isolated 3 times, and
557 amplified as described below.
558
559 Phages were propagated by picking a single phage plaque into a liquid culture of *B. subtilis* BEST7003
560 grown at 37 °C to OD_{600} of 0.3 in MMB broth until culture collapse (or three hours in case of no lysis).
561 The culture was then centrifuged for 10 min at 3200 *g* and the supernatant was filtered through a 0.45 µm
562 filter to get rid of remaining bacteria and bacterial debris.
563
564 High titer phage lysates (>10^7 pfu ml^{-1}) were used for DNA extraction. 500 µl of the phage lysate was
565 treated with DNase-I (Merck cat #11284932001) added to a final concentration of 20 mg ml^{-1} and
566 incubated at 37 °C for 1 hour to remove bacterial DNA. DNA was extracted using the QIAGEN DNeasy
567 blood and tissue kit (cat #69504) starting from the Proteinase-K treatment step.
568
569 Phages from the SBSphiJ and SPbeta groups were sequenced using a modified Nextera protocol as
570 previously described[58]. Following Illumina sequencing, adapter sequences were removed from the reads
571 using Cutadapt version 2.8 [59] with the option -q 5. The trimmed reads from each phage genome were
572 assembled into scaffolds using SPAdes genome assembler version 3.14.0 [60], using the –careful flag.
573
574 The genomes of phages from the SPO1 group were sequenced via a long-read PacBio method, due to the
575 high amount of modified bases in these phages. For library construction of phages from the SPO1 group, 1
576 µg of genomic DNA samples was fragmented using g-tubes (Covaris). Sheared DNA was purified with
577 AMPure PB beads and was used to construct a SMRTbell library according to the PacBio library
578 construction guidelines[61]. Samples were barcoded using Barcoded Overhang Adapters and pooled to one
579 final library. Quantity and quality of the SMRTbell library were determined using the Qubit HS DNA kit
580 and Agilent TapeStation Genomic DNA. No size selection was performed. The PacBio sequencing primer
581 was then annealed to the SMRTbell library followed by binding of the polymerase to the primer–library
582 complex. The library was loaded onto one SMRT cell in the PacBio Sequel system and sequenced in a
583 Continuous Long Read (CLR) mode at a 10 h movie time.
584
585 All phage genomes sequenced and assembled in this study were analyzed with Prodigal version 2.6.3 [62]
586 (default parameters) to predict ORFs.
587
588 <u>Plaque assays</u>
589
590 Phage titer was determined using the small drop plaque assay method[63]. 400 µl of overnight culture of
591 bacteria were mixed with 0.5% agar and 30 ml MMB and poured into a 10 cm square plate followed by
592 incubation for 1 h at RT. In cases of bacteria expressing anti-defense candidates and in the experiment

593 with phage SBSphiJ with a Tad2 knock-in, 1 mM IPTG was added to the 30 ml MMB 0.5% agar. In cases
594 of bacteria expressing dCas9-gRNA constructs, 0.002% xylose was added to the medium.10-fold serial
595 dilutions in MMB were performed for each of the tested phages and 10 µl drops were put on the bacterial
596 layer. After the drops had dried up, the plates were inverted and incubated at RT overnight. Plaque forming
597 units (PFUs) were determined by counting the derived plaques after overnight incubation and lysate titer
598 was determined by calculating PFUs per ml. When no individual plaques could be identified, a faint lysis
599 zone across the drop area was considered to be 10 plaques. Efficiency of plating (EOP) was measured by
600 comparing plaque assay results on control bacteria and bacteria containing the defense system and/or a
601 candidate anti-defense gene.
602
603 Prediction of candidate anti-defense genes
604
605 Predicted protein sequences from all phage genomes in each phage family were clustered into groups of
606 homologs using the cluster module in MMSeqs2 release 12-113e3 [64], with the parameters -e 10, -c 0.8, -s
607 8, --min-seq-id 0.3 and the flag --single-step-clustering. For each defense system, anti-defense candidates
608 were defined as clusters that have a representation in all the phages that overcome the defense system and
609 are absent from all the phages that are blocked by the defense system. One member was chosen from each
610 cluster as a candidate anti-defense gene for further experimental testing (Supplementary table 7). In the
611 case of the Hachiman defense system, only predicted genes with no known function were tested
612 experimentally. *Gad2* was predicted based on its localization in the sane locus as *gad1* in phages SPbetaL6
613 and SPbetaL7.
614
615 Cloning of candidate anti-defense genes
616
617 The DNA of each anti-defense candidate was amplified from the source phage genome using KAPA HiFi
618 HotStart ReadyMix (Roche cat # KK2601) and primers provided in Supplementary table 7, and cloned
619 using the NEBuilder HiFI DNA Assembly cloning kit (NEB, no. E5520S) into the pSG-*thrC*-Phspank
620 vector. Homologs of verified anti-defense genes (Supplementary tables 8,10,12 and 14) were synthesized
621 and cloned by Genscript Corp. The anti-defense candidates were cloned into the pSG-*thrC*-Phspank
622 vector[33] and transformed into NEB 5-alpha competent cells. The cloned vector was subsequently
623 transformed into *B. subtilis* BEST7003 cells containing the respective defense systems as applicable
624 integrated into the *amyE* locus[18], resulting in cultures expressing both defense system and their
625 corresponding anti-defense gene candidates, integrated into the *amyE* and *thrC* loci, respectively. As a
626 negative control, a transformant with an identical plasmid containing sfGFP instead of the anti-defense
627 gene, was used. Transformation to *B. subtilis* was performed using MC medium as previously described[18]
628 and plated on LB agar plates supplemented with 5 µg ml^{-1} chloramphenicol incubated overnight at 30 °C.
629 Whole-genome sequencing was then applied to all transformed *B. subtilis* strains, and Breseq (version
630 0.34.1) analysis[65] was used to verify the integrity of the inserts and lack of mutations.
631
632 Gad1 knockout in phi3T lysogenic strain
633
634 The upstream and downstream homologous arms of Gad1 were amplified from the phi3T phage genome
635 using the PCR primer pairs Gad1_AF and Gad1_AR, and Gad1_BF and Gad1_BR, respectively
636 (Supplementary table 15). The spectinomycin resistance gene cassette was amplified from the vector
637 pJmp3 (addgene plasmid #79875) using the PCR primers Spec_F and Spec_R (Supplementary table 15).
638 The pJmp3 backbone was amplified using the primers Vector_F and Vector_R (Supplementary table 15).

These three parts were assembled together with the pJmp3 backbone using the NEBuilder HiFi DNA Assembly cloning kit (NEB cat # E5520S) and transformed to *E. coli* NEB 5-alpha competent cells. The cloned vector was then transformed into the phi3T lysogenic strain (BGSCID 1L1) using MC medium[18] and was plated on LB agar plates supplemented with 100 µg ml^{-1} spectinomycin and incubated overnight at 30 °C. The modified phi3T prophage was induced from the lysogenic bacterial strain grown to an OD_{600} of 0.3 by the addition of 0.5 µg ml^{-1} Mitomycin C (Sigma, M0503). After 3 h, the culture was centrifuged for 10 min at 3200 *g* and the supernatant containing the modified phages was collected and filtered through 0.2 µm filters. Whole-genome sequencing was performed to verify the sequence of the modified phage.

Gad2 knockout in SPbetaL7 using Cas13a

Cas13a was amplified from the pBA559 plasmid[66] with the primers cas13a_fwd and cas13a_rev. The xylose promoter and homology arms for integration into the thrC site were amplified from plasmid pJG_thrC_dCAS9_gRNA[33] with primers dcas9xylProm_fwd and dcas9xylProm_rev. The gRNA complimentary to the beginning of Gad2 was amplified from the pBA559 plasmid with primers gRNAcas13_fwd and gRNAcas13L7159_rev. Plasmid assembly was conducted using NEBuilder HiFi DNA Assembly cloning kit (NEB, cat # E5520S) and transformed to NEB 5-alpha -competent cells. The cloned vector was subsequently transformed into the thrC site of *B. subtilis* BEST7003.

For the selection of Gad2 knockout SPbetaL7 phages, overnight culture of the Cas13a-gRNA containing bacteria was mixed was diluted 1:100 with MMB agar 0.5% with 0.2% xylose, and grown for 1 hour at RT. Then, 10^8 PFU of phage SPbetaL7 were spread on the plate. On the next day, several individual plaques were collected and propagated with 1 ml of the Cas13a-gRNA containing bacteria. Gad2 knockout was verified using PCR primers L7159Fchk and L7159Rchk. Sequencing of the product demonstrated deletion of bases 109,505-110,753 from the SPbetaL7 genome, spanning the entire Gad2 gene and as well as the Gad2 promoter. The selected knockout phage was purified three times on *B. subtilis* BEST7003.

Gabija / Gabija + Gad1 complex assembly and *in vitro* nuclease activity

*Bc*GajAB and *Bc*GajAB + *Shewanella sp*. phage 1/4 Gad1 complexes were purified as described (Antine et al. 2023 submitted manuscript). A 56-bp dsDNA with a sequence specific motif derived from phage Lambda (5′- TTTTTTTTTTTTTTTTTAATAACCCGGTTATTTTTTTTTTTTTTTTTTTTTTT-3′)[40] was pre-incubated with purified GajAB or GajAB + Gad1 in 20 µL DNA cleavage reactions containing 1 µM dsDNA, 1 µM GajAB or GajAB + Gad1, 1mM $MgCl_2$, 20 mM Tris-HCl pH 9.0 for 1, 5, 10, 15, and 20 min at 37 °C. Following incubation, reactions were stopped with DNA loading buffer containing EDTA and 10 µL was analyzed on a 2% TB (Tris-borate) agarose gel. Gels were run at 250V for 40 min at 4 °C, then stained by rocking at room-temperature in TB buffer with 10 µg ml^{-1} ethidium bromide for 30 min. Gels were de-stained in TB buffer for 40 min and imaged with a ChemiDoc MP Imaging System.

Gad2 pulldown assay

684
685 GajA, GajB, and Gad1 proteins were co-expressed together using custom pET vector with an N-terminal
686 6×His-SUMO2-5×GS tag on GajA and ribosome binding site between GajA and GajB, and GajB and
687 Gad1. *Brevibacillus laterosporus* Gad2 was cloned from synthetic DNA (Integrated DNA Technologies)
688 into a custom pBAD vector containing a chloramphenicol resistance gene and an IPTG-inducible promoter
689 or a custom pET vector with an N-terminal 6×His-SUMO2 tag. Plasmids were transformed and expressed
690 in BL21(DE3) or LOBSTR-BL21(DE3)-RIL (Kerafast) cells and subject to Ni-NTA column
691 chromatography and SUMO2 cleavage with SENP2. Gad2 pulldown was analyzed by SDS-PAGE and
692 Coomassie Blue staining.
693
694 GajAB DNA-Gad2 cleavage assay
695
696 GajAB complex was expressed and purified as previously described[42]. Briefly, Gad2 was expressed with
697 an N-terminal 6×His-SUMO2 tag in LOBSTR-BL21(DE3)-RIL cells (Kerafast) and purified using Ni-
698 NTA resin (Qiagen) followed by size exclusion chromatography using a 16/600 Superdex 200 column
699 (Cytiva). The same 56-bp dsDNA substrate as used in GajAB DNA cleavage assays was incubated with
700 1 μM, 4 μM, or 8 μM Gad2 in a 20 μL DNA cleavage reaction containing 0.5 μM NAD+ (Sigma
701 Aldrich), 0.5 μM NTPs, 1 μM dsDNA, 1 mM MgCl2, 20 mM Tris-HCl pH 9.0 for 10 min on ice. 1 μM
702 GajAB was added to the reaction and incubated for 20 min at 37 °C. A control Gad2 only lane was run
703 to demonstrate slight nucleic acid contamination within the Gad2 protein prep. Following incubation,
704 reactions were terminated with DNA loading buffer containing 60 mM EDTA and 10 μL was analyzed
705 on a 2% TB agarose gel run at 250 V for 30 min. The gel was post-stained by rocking at room
706 temperature with TB buffer containing 10 μg ml−1 ethidium bromide, de-stained in TB buffer alone for
707 30 min, and imaged on a ChemiDoc MP Imaging System.
708
709 Construction of dCas9 and gRNA cassettes for integration in *B. subtilis thrC* site
710
711 The plasmid pJG_thrC_dCAS9_gRNA was constructed as previously described[33]. To insert new spacers,
712 two fragments were amplified from pJG_thrC_dCAS9_gRNA and the new spacer was introduced into the
713 overlap of primers designed for NEBuilder HiFi DNA Assembly (NEB, no. E5520S). For the gRNA used
714 to target *tad2*, the first fragment was amplified using primers JG528 and JG525, and the second using
715 primers JG529 and JG524 (Supplementary table 15). The resulting assembled construct had the gRNA
716 sequence "aagatgatgttcccaaacac". For the gRNA used to target *had1*, the first fragment was amplified
717 using primers JG389 and JG381, and the second using primers JG390 and JG382 (Supplementary table
718 15). The resulting assembled construct had the gRNA sequence "gcttgctaggattagtgtcc". The gRNA
719 sequence "ctatgattgatttttttagc" was used as a control. It was constructed as mentioned above, with primers
720 JG389 and JG378, and JG390 and JG388 (Supplementary table 15). Shuttle vectors were propagated in *E.*
721 *coli* NEB 5-alpha with 100 μg ml^{-1} ampicillin selection. Plasmids were isolated from *E. coli* NEB 5-alpha
722 before transformation into the appropriate *B. subtilis* BEST7003 strains. The vectors containing the
723 dCas9–gRNA sequences were cloned to *B. subtilis* strains containing the respective defense system, as
724 well as to a control strain lacking the defense system.
725
726 Knock-in of Had1 and Tad2 into phage SBSphiJ and Gad1 into phage SPbeta
727
728 The DNA sequence of *tad2*, together with the Phspank promoter, was amplified from the Tad2-containing
729 pSG-*thrC*-Phspank plasmid using KAPA HiFi HotStart ReadyMix (Roche, cat #KK2601) with the primer

730 pair tad2KIF and tad2KIr (Supplementary table 15). The DNA sequence of *had1*, together with its
731 upstream intergenic region, was amplified from the genome of phage SBSphiJ4 with the primer pair
732 had1KIF and had1KIR (Supplementary table 15). The backbone fragment with the upstream and
733 downstream genomic arms (±1.2 kbp) for the integration site of *tad2* and *had1* was amplified from the
734 plasmid used previously for knock-in of the *tad1* gene[33], with the primer pair backboneKIF and
735 backboneKIR (Supplementary table 15). The DNA sequence of *gad1*, together with its upstream
736 intergenic region, was amplified from the genome of phage phi3T with the primer pair gad1KIF and
737 gad1KIR (Supplementary table 15). The upstream and downstream genomic arms (±1.2 kbp) for the
738 integration site of the *gad1* gene within the SPbeta genome were amplified from the genome of phage
739 SPbeta using the primer pair gad1LFF and gad1LFR, and the primer pair gad1RFF and gad1LRR
740 (Supplementary table 15). Cloning was conducted using the NEBuilder HiFi DNA Assembly cloning kit
741 (NEB, no. E5520S) and transformed to NEB 5-alpha-competent cells. The cloned vector was subsequently
742 transformed into the *thrC* site of *B. subtilis* BEST7003.
743
744 The *tad2*, *had1* and *gad1* containing *B. subtilis* BEST7003 strains were then infected with phages SBSphiJ
745 (*tad2* and *had1*) or SPbeta (*gad1*) with an MOI of 0.1 and cell lysates were collected. Tad2 lysate was
746 used to infect a Thoeris-containing *B. subtilis* culture in two consecutive rounds with an MOI of 2 in each
747 round (30 °C, 1mM IPTG). Had1 lysate was used to infect a Hachiman-containing *B. subtilis* culture in
748 two consecutive rounds with an MOI of 2 in each round (25 °C). Gad1 lysate was used to infect a Gabija-
749 containing *B. subtilis* culture in two consecutive rounds with an MOI of 2 in each round (25 °C). Several
750 plaques were collected and screened using PCR for the desired insertion within the phage genome. Phages
751 with anti-defense genes were purified three times on *B. subtilis* BEST7003. Purified phages were verified
752 again for the presence of *tad2*, *had1* and *gad1* using PCR amplifications.
753
754 <u>Identification of anti-defense homologs and phylogenetic reconstruction</u>
755
756 Homologs of anti-defense genes were searched in the metagenomic gut virus (MGV)[46] database using the
757 "search" option of MMseqs release 12-113e3 with default parameters. Homologs of Gad1, Gad2 and Had1
758 were searched in the integrated microbial genomes (IMG) database[45] using the blast option in the IMG
759 web server. Gad1 and Gad2 homologs were searched using the default parameters, while Had1 homologs
760 were searched using an e-value of 10 due to their short size. For Gad1 and Had1 this process was repeated
761 iteratively for homologs that were found, until convergence. For Tad2, due to the multitude of homologs,
762 homology search was done using the "search" option of MMseqs release 12-113e3 with default
763 parameters, against ~38000 prokaryotic genomes downloaded from the IMG database in October 2017.
764
765 For each family of anti-defense proteins, the unique (non-redundant) sequences were used for multiple
766 sequence alignment with MAFFT version 7.402 [67] using default parameters. Phylogenetic trees were
767 constructed using IQ-TREE version 1.6.5 [68] with the -m LG parameter. The online tool iTOL24 (v.5)[69]
768 was used for tree visualization. Phage family annotations were based on the prediction in the MGV
769 database. The host phyla annotations were either based on the prediction in the MGV database, or the
770 IMG taxonomy of the bacteria in which the prophage was found. Gabija and Thoeris defense systems
771 were found in the bacterial genomes using DefenseFinder[39] version 1.0.9 and database release 1.2.3.
772
773
774
775

776 Preparation of filtered cell lysates
777
778 For generating filtered cell lysates, we used *B. subtilis* BEST7003 cells co-expressing Tad2 and the *B.*
779 *cereus* MSX-D12 Thoeris system in which ThsA was inactivated (ThsB/ThsA$_{N112A}$). Tad2 was integrated
780 in the thrC locus as described above and expressed from an inducible Phspank promoter, and the Thoeris
781 system was integrated in the amyE locus and expressed from its native promoter as described above.
782 Controls included cells expressing only the ThsB/ThsA$_{N112A}$ Thoeris system without Tad2, as well as cells
783 lacking both the Thoeris system and Tad2. These cultures were grown overnight and then diluted 1:100
784 in 250 ml MMB medium supplemented with 1 mM IPTG and grown at 37 °C, 200 rpm shaking
785 for 120 min followed by incubation and shaking at 25 °C, 200 rpm until reaching an OD_{600} of 0.3. At this
786 point, a sample of 40 ml was taken as the uninfected (time 0 min) sample, and SBSphiJ phage was added
787 to the remaining 210 ml culture at an MOI of 10. Flasks were incubated at 25 °C with shaking (200 rpm),
788 for the duration of the experiment. 40 ml samples were collected at time points 75, 90, 105 min post-
789 infection. Immediately upon sample removal (including time point 0 min), the 40 ml sample tubes were
790 centrifuged at 4 °C for 10 min at 3200 *g* to pellet the cells. The supernatant was discarded, and the pellet
791 was flash frozen and stored at −80 °C.
792
793 To extract cell metabolites from frozen pellets, 600 µl of 100 mM Na phosphate buffer (pH 8.0) was added
794 to each pellet. Samples were transferred to FastPrep Lysing Matrix B in a 2 ml tube (MP Biomedicals, no.
795 116911100) and lysed at 4 °C using a FastPrep bead beater for 2×40 s at 6 m s^{-1}. Tubes were then
796 centrifuged at 4 °C for 10 min at 15,000 *g*. Supernatant was then transferred to an Amicon Ultra-0.5
797 Centrifugal Filter Unit 3 kDa (Merck Millipore, no. UFC500396) and centrifuged for 45 min at 4 °C,
798 12,000 *g*. Filtered lysates were taken for *in vitro* ThsA-based NADase activity assay.
799
800 Expression and purification of ThsA
801
802 *B. cereus* MSX-D12 *thsA* fused to a C-terminal TwinStrep tag was cloned into a pACYC-Duet1 plasmid
803 (addgene plasmid #71147). The protein was expressed under the control of the T7 promoter together with
804 a C-terminal Twin-Strep tag for subsequent purification. Expression was performed in 5 L LB medium
805 supplemented with chloramphenicol (34 mg ml^{-1}) in *E. coli* BL21(DE3) cells. Induction was performed
806 with 0.2 mM IPTG at 15 °C overnight. The cultures were collected by centrifugation and lysed by a cooled
807 cell disrupter (Constant Systems) in 100 ml lysis buffer composed of 20 mM HEPES pH 7.5, 0.3 M NaCl,
808 10% glycerol and 5 mM β-mercaptoethanol, 200 KU/100 ml lysozyme, 20 µg ml^{-1} DNase, 1 mM $MgCl_2$,
809 1 mM phenylmethylsulfonyl fluoride (PMSF) and protease inhibitor cocktail (Millipore, 539134). Cell
810 debris were sedimented by centrifugation, and the lysate supernatant was incubated with 2 ml washed
811 StrepTactin XT beads (IBA, 2-5030–025) for 1 h at 4 °C. The sedimented beads were then packed into a
812 column connected to an FPLC allowing the lysate to pass through the column at 1 ml min^{-1}. The column
813 was washed with 20 ml lysis buffer. ThsA was eluted from the column using elution buffer containing 50
814 mM biotin, 100 mM Tris pH 8, 150 mM NaCl and 1 mM EDTA. Peaks containing the ThsA protein were
815 injected to a size-exclusion chromatography (SEC) column (Superdex 200_16/60, GE Healthcare, 28-
816 9893-35) equilibrated with SEC buffer (20 mM HEPES pH 7.5, 200 mM NaCl and 2 mM DTT). Peaks
817 were collected from the SEC column, aliquoted and frozen at −80 °C to be used for subsequent
818 experiments.
819
820
821

822 ThsA-based NADase activity assay
823
824 NADase reaction was performed in black 96-well half area plates (Corning, 3694). In each reaction
825 microwell, purified ThsA protein was added to cell lysate, or to in vitro reactions of Tad2 with 1″–3′
826 gcADPR, or to 100 mM sodium phosphate buffer pH 8.0. 5 µl of 5 mM nicotinamide 1,N6-ethenoadenine
827 dinucleotide (εNAD^+, Sigma, N2630) solution was added to each well immediately before the beginning
828 of measurements, resulting in a final concentration of 100 nM ThsA protein in a 50 µl final volume
829 reaction. Plates were incubated inside a Tecan Infinite M200 plate reader at 25 °C, and measurements
830 were taken at 300 nm excitation wavelength and 410 nm emission wavelength. Reaction rate was
831 calculated from the linear part of the initial reaction.
832
833 Tad2 protein cloning, expression, and purification for biochemistry
834
835 The SPO1 *tad2* gene was cloned into the expression vector pET28-bdSumo as described previously[33].
836 Tad2 was expressed in *E. coli* BL21(DE3) by induction with 200 µM IPTG at 15 °C overnight. A 2 L
837 culture of bacteria expressing Tad2 was harvested and lysed by a cooled cell disrupter (Constant Systems)
838 in lysis buffer (50mM Tris pH 8, 0.25M NaCl, 10% Glycerol) containing 200KU 100 ml^{-1} lysozyme,
839 20ug ml^{-1} DNase, 1mM $MgCl_2$, 1 mM phenylmethylsulfonyl fluoride (PMSF) and protease inhibitor
840 cocktail. After clarification of the supernatant by centrifugation, the lysate was incubated with 5 ml
841 washed Ni beads (Adar Biotech) for 1 h at 4 °C. After removing the supernatant, the beads were washed
842 4 times with 50 ml lysis buffer. Tad2 was eluted by incubation of the beads with 10 ml cleavage buffer
843 (50 mM Tris pH 8, 0.25M NaCl, 10% Glycerol and 0.4 mg bdSumo protease) for 1 h at 23 °C. The
844 supernatant, containing cleaved Tad2, was removed, and an additional 5 ml cleavage buffer was added to
845 the beads and left overnight at 4 °C. The two elution solutions were combined, concentrated, and applied
846 to a size exclusion (SEC) column (HiLoad_16/60_Superdex75 prep-grade, Cytiva) equilibrated with 50
847 mM Tris pH 8, 100 mM NaCl. Pure Tad2 migrating as a single peak was pooled and flash frozen in
848 aliquots using liquid nitrogen and stored at −80 °C.
849
850 Incubation of purified 1″–3′ gcADPR with Tad2
851
852 2.4 µM purified Tad2 was incubated with 600 nM of 1″–3′ gcADPR in 100 mM Na Phosphate buffer, pH
853 8.0 for 10 min, at 25°C, followed by an additional 10 min incubation at either 95°C or 25°C. Following
854 incubation, samples were left on ice for 1 min. The samples were then used for ThsA-based NADase
855 activity assays as described above.
856
857 Analytical SEC analysis of apo and ligand bound Tad2
858
859 50 µl of Tad2 (158 µM) was incubated with 30 µl of 1 mM 1″–3′ gcADPR at 25 °C, in 0.1 M NaCl, 50
860 mM TrisHCl pH 8.0, for 20 min. The incubated mixture, and an apo protein incubated with an identical
861 buffer without the ligand, were then loaded on a size exclusion Superdex_200_10/300 analytical column
862 (PBS buffer) and monitored for absorption at both 260_{nm} and 280_{nm}. The oligomeric nature of Tad2 apo
863 protein was evaluated by comparing the retention time of apo-Tad2 to that of five internal standard
864 proteins (Ribonuclease 13.7 kD, Chymotrypsin 25 kD, BSA 66 kD, Aldolase 160 kD, and apoferritin 443
865 kD) using a size exclusion Superdex_200_10/300.
866
867 Surface Plasmon Resonance (SPR) measurements of Tad2 binding to 1″–3′ gcADPR and cADPR

868
869 Binding of 1″–3′ gcADPR to Tad2 was monitored by surface plasmon resonance with a BIAcore S200
870 apparatus (Cytiva, Sweden). Tad2 was immobilized on a CM5 S Series chip (Cytiva, Sweden) by amine
871 coupling chemistry using the following protocol: chip activation was carried out with a freshly prepared
872 mixture of N-hydroxysuccinimide (50 mM in water) and 1-ethyl-3-(3-dimethylaminopropyl)
873 carbodiimide (195 mM in water) for 7.5 min in DPBS (Sartorius, SKU 02-023-5A) (flow rate of 10
874 µl/min). DPBS served as the running buffer along the experiment. Tad2 protein (5 µg ml^{-1} in 150 mM
875 sodium acetate buffer, pH 3.8) was injected for 5 min (flow rate 10 µl/min) and the remaining activated
876 carboxylic groups were blocked by injecting of 1 M ethanolamine hydrochloride, pH 8.0, for 5 min (flow
877 rate 10 µl/min). Subsequently, a total of 1,800 RU (Response Units) of Tad2 were immobilized on to the
878 chip. Before data collection, a normalization cycle followed by a priming cycle were run to stabilize the
879 instrument. Binding of 1″–3′ gcADPR to Tad2 was monitored by injecting 1″–3′ gcADPR at multiple
880 concentrations for 2 min at 25 °C and flow rate of 50 µl/min. Dissociation was carried out for 180 sec. No
881 regeneration step was required after ligand binding as the dissociation reached baseline spontaneously.
882 Sensograms were fit to a 1:1 binding model (S200 evaluation software 1.1) which yielded the kinetic
883 constants (ka and kd) of the interaction. kd divided by ka yield the steady state KD. cADPR which served
884 as a control did not bind, as expected.
885
886 Protein cloning, expression, and purification
887
888 Synthetic DNA fragments (Integrated DNA Technologies) of cmTad1, $AbTIR^{TIR}$ (Δ1–156), cbTad1,
889 SPO1 Tad2 and *Bacillus toyonensis* Had1 genes were cloned into a custom pET expression vector
890 containing an N-terminal 6×His-SUMO2 tag and an ampicillin resistance gene by Gibson assembly, as
891 previously described[70]. Three colonies of BL21(DE3) RIL *E. coli* transformed with these plasmids and
892 grown on MDG agar plates (1.5% agar, 2 mM $MgSO_4$, 0.5% glucose, 25 mM Na_2HPO_4, 25 mM KH_2PO_4,
893 50 mM NH_4Cl, 5 mM Na_2SO_4, 0.25% aspartic acid, 2–50 µM trace metals) were picked into a 30 ml MDG
894 starter culture and shaken overnight at 230 rpm and 37 °C. A 1 L culture of M9ZB expression medium
895 (2 mM $MgSO_4$, 0.5% glycerol, 47.8 mM Na_2HPO_4, 22 mM KH_2PO_4, 18.7 mM NH_4Cl, 85.6 mM NaCl,
896 1% Cas-amino acids, 2–50 µM trace metals, 100 µg ml^{-1} ampicillin and 34 µg ml^{-1} chloramphenicol) was
897 seeded with 15 ml starter culture and grown at 230 rpm and 37 °C to an OD_{600} of 2 before induction of
898 expression with 0.5 mM IPTG and incubation at 230 rpm and 16°C for 16 hours. For $AbTIR^{TIR}$ expression,
899 nicotinamide-supplemented 2YT expression medium (1.6% w/v tryptone, 1% w/v yeast extract, 342 mM
900 NaCl, 10 mM NAM, 100 µg ml^{-1} ampicillin, 34 µg ml^{-1} chloramphenicol) was used instead. Cells were
901 harvested by centrifugation, resuspended in lysis buffer (20 mM HEPES-KOH pH 7.5, 400 mM NaCl,
902 30 mM imidazole, 10% glycerol, 1 mM DTT), lysed by sonication, and clarified by centrifugation at
903 25,000*g* for 20 min. Lysate was passed over 8 ml Ni-NTA resin (Qiagen), washed with 70 ml wash buffer
904 (20 mM HEPES-KOH pH 7.5, 1 M NaCl, 30 mM imidazole, 10% glycerol, 1 mM DTT), eluted with lysis
905 buffer supplemented to 300 mM imidazole, and dialyzed in 14 kDa dialysis tubing in dialysis buffer
906 (20 mM HEPES-KOH pH 7.5, 250 mM KCl, 1 mM DTT) overnight at 4°C with purified human SENP2
907 for 6× His-SUMO2 tag cleavage. For crystallography, proteins were further purified on a Superdex 75
908 16/600 size-exclusion chromatography column (Cytiva). Final samples were concentrated to >20 mg ml^{-1},
909 flash frozen, and stored at −80°C.
910
911 ThsB′ was cloned and purified similarly as described above, except that it was cloned into a custom pET
912 vector containing a C-terminal 6× His tag and a chloramphenicol resistance gene, transformed into

913 BL21(DE3) cells, grown in the presence of chloramphenicol only, expressed in 2YT medium with 10 mM
914 NAM, and concentrated to 4 mg ml^{-1} after dialysis before flash-freezing and storage.
915
916 1″–2′ gcADPR and 1″–3′ gcADPR production and purification
917
918 gcADPR molecules were produced as described previously[33]. For 1″–2′ gcADPR production, purified
919 $AbTIR^{TIR}$, a bacterial enzyme that efficiently converts NAD^+ to 1″–2′ gcADPR[50], was used to set up 300µl
920 reactions (50 mM HEPES-KOH, 150 mM NaCl, 20 mM NAD^+, 40 µM $AbTIR^{TIR}$). For 1″–3′ gcADPR
921 production, Purified ThsB'[33] was used to set up 50 ml reactions (50 mM HEPES-KOH pH 7.5, 150 mM
922 NaCl, 2 mM NAD^+, 16 µM ThsB'). Reactions were carried out at RT for 24-48 hours before boiling at 95
923 °C for 10 min, pelleting at 13,500 *g* for 20 min, and filtering through a 10 kDa MWCO filter (Amicon).
924 For the $AbTIR^{TIR}$ reaction, filtrate was diluted to 30 ml with PBS followed by addition of 200 µM purified
925 cmTad1. For the ThsB' reaction, 10 µM purified cmTad1 was added directly to 50 ml of filtrate. Mixtures
926 were then incubated for 1 hour at RT to allow cmTad1–gcADPR complex formation. The complexes were
927 washed by successive concentration and dilution in a 10 kDa MWCO filter first with five 1:20 dilutions
928 in PBS followed by five 1:20 washes in water. Complexes were concentrated to >3 mM before final
929 release and extraction of gcADPR by boiling at 95 °C for 10 min, pelleting at 13,500 *g* for 20 min, filtering
930 through a 3 kDa MWCO filter, and collecting the filtrate. Final purity and concentration were assessed by
931 HPLC.
932
933 Protein crystallization and structural analysis
934
935 cbTad1, SPO1 Tad2, and Had1 crystals were grown by the hanging-drop method in EasyXtal 15-well
936 trays (NeXtal) at 16°C. Hanging-drops were set using 1 µl of diluted protein solution (5–10 mg ml^{-1}
937 protein, 20 mM HEPES-KOH pH 7.5, 70–80 mM KCl, 1 mM TCEP) and 1 µl reservoir solution over a
938 400µl well of reservoir solution. Proteins were crystallized and cryoprotected under the following
939 conditions before being harvested by flash-freezing in liquid nitrogen: (1) cbTad1 complexed with 1″–3′
940 gcADPR: Crystals were grown for 3 weeks in drops supplemented with 500 µM ThsB′-derived 1″–3′
941 gcADPR using reservoir solution containing 0.2 M $MgCl_2$, 0.1 M Tris-HCl pH 8.5, and 3.4 M 1,6-
942 hexanediol. (2) SPO1 Tad2 in the apo state: Crystals were grown for 1 week using reservoir solution
943 containing 0.1 M 2-(*N*-morpholino) ethanesulfonic acid pH 6.5, 10% (v/v) 1,4-dioxane, and 1.6 M
944 ammonium sulfate before being cryoprotected with reservoir solution supplemented with 25% (v/v)
945 glycerol. (3) SPO1 Tad2 complexed with 1″–3′ gcADPR: Crystals were grown for 1 week in drops
946 supplemented with 500 µM ThsB′-derived 1″–3′ gcADPR using reservoir solution containing 0.2 M
947 magnesium nitrate and 18% (w/v) PEG 3350 before being cryoprotected with reservoir solution
948 supplemented with 20% (v/v) ethylene glycol and 1 mM 1″–3′ gcADPR. (4) SPO1 Tad2 complexed with
949 1″–2′ gcADPR: Crystals were grown for 1 week in drops supplemented with 500 µM $AbTIR^{TIR}$-derived
950 1″–2′ gcADPR using reservoir solution containing 0.1 M Tris-HCl pH 8.5, 12% (v/v) glycerol, and 1.5 M
951 ammonium sulfate before being cryoprotected with reservoir solution supplemented with 15% (v/v)
952 ethylene glycol and 1 mM 1″–2′ gcADPR. (5) Had1 in the apo state: Crystals were grown for 1 week
953 using reservoir solution containing 100 mM MES pH 6.2 and 30% PEG 4000 before being cryoprotected
954 with reservoir solution supplemented with 10% (v/v) ethylene glycol.
955
956 CbTad1 and SPO1 Tad2 X-ray diffraction data were collected at the Advanced Photon Source (beamline
957 24-ID-C), and data were processed with XDS[71] and Aimless[72] using the SSRL autoxds script (A.
958 Gonzalez, Stanford SSRL). Phases were determined by molecular replacement in Phenix using either

959 previously determined cbTad1 structures[33] (PDB 7UAV, 7UAW) or sequence-predicted SPO1 Tad2
960 truncated structures from ColabFold v1.5.2 [73]. Model building was performed in Coot[74], refinement was
961 performed in Phenix[75]. Had1 X-ray diffraction data were collected at the Advanced Light Source
962 (beamline 8.2.1) and data were processed with XDS[71] and Aimless[72] using the SSRL autoxds script (A.
963 Gonzales, Stanford, SSRL). Experimental phase information was determined by molecular replacement
964 using a dimeric Had1 AlphaFold2 predicted structure[73] in Phenix[75]. Model building was completed in
965 Coot[74] and then refined in Phenix[75]. Statistics were analyzed as presented in Extended Data Table 1[76–78],
966 and structure figures were produced in PyMOL. Final structures were refined to stereochemistry statistics
967 for Ramachandran plot (favored/allowed), rotamer outliers and MolProbity score as follows: cbTad1–1″–
968 3′-gcADPR, 95.88/4.12%, 0.92%, 1.47; SPO1 Tad2 apo, 96.15/2.56%, 0.74%, 1.59; SPO1 Tad2–1″–3′-
969 gcADPR, 99.18/0.82%, 1.5%, 1.33; SPO1 Tad2–1″–2′-gcADPR, 99.36/0.64%, 2.19%, 1.27; Had1,
970 96.18/3.82%, 0.69%, 1.20.
971
972 HPLC analysis of Tad2 incubation with 1″–3′ gcADPR
973
974 Reactions to analyze cleavage of 1″–3′ gcADPR were performed in 120 µl reactions consisting of 50 mM
975 Tris-HCl pH 7.5, 100 mM KCl, 5 mM $MgCl_2$, 1 mM $MnCl_2$, 50 µM gcADPR isomer, and either buffer or
976 1 µM Tad2. As a control, 1″–3′ gcADPR was also incubated with 1 µl Cap-Clip Acid Pyrophosphatase
977 (known to cleave diphosphate linkages on mRNA caps, Fisher Scientific), using the manufacturer's
978 recommended reaction conditions. Reactions were incubated at 37 °C for 1 h before filtration using a 3
979 kDa MWCO filter. Filtered reactions were analyzed using a C18 column (Agilent Zorbax Bonus-RP 4.6
980 x 150 mm) heated to 40 °C and run at 1 ml min^{-1} using a buffer of 50 mM NaH_2PO_4-NaOH pH 6.8
981 supplemented with 3% acetonitrile.
982
983 **Extended References**
984
985 57. A. M. Kropinski, A. Mazzocco, T. E. Waddell, E. L. & Johnson, R. P. methods and protocols. in
986 *Bacteriophages* 69–76 (Humana Press, 2009).
987 58. Baym, M. *et al.* Inexpensive multiplexed library preparation for megabase-sized genomes. *PLoS*
988 *One* **10**, e0128036 (2015).
989 59. Martin, M. Cutadapt removes adapter sequences from high-throughput sequencing reads.
990 *EMBnet.journal* **17**, 10 (2011).
991 60. Nurk, S. *et al.* Assembling Genomes and Mini-metagenomes from Highly Chimeric Reads. in
992 *Research in Computational Molecular Biology* 158–170 (2013).
993 61. Procedure & Checklist – Preparing Multiplexed Microbial Libraries Using SMRTbell Express
994 Template Prep Kit 2.0. https://www.pacb.com/wp-content/uploads/Procedure-Checklist-–-
995 Preparing-Multiplexed-Microbial-Libraries-Using-SMRTbell-Express-Template-Prep-Kit-
996 2.0.pdf.
997 62. Hyatt, D. *et al.* Prodigal: prokaryotic gene recognition and translation initiation site identification.
998 *BMC Bioinformatics* **11**, 119 (2010).
999 63. A. Mazzocco, T. E. Waddell, E. Lingohr, R. P. J. Enumeration of Bacteriophages Using the Small
1000 Drop Plaque Assay System. in *Bacteriophages* 81–85 (Humana Press, 2009).
1001 64. Steinegger, M. & Söding, J. MMseqs2 enables sensitive protein sequence searching for the
1002 analysis of massive data sets. *Nat. Biotechnol.* **35**, 1026–1028 (2017).
1003 65. Deatherage, D. E. & Barrick, J. E. Identification of mutations in laboratory-evolved microbes
1004 from next-generation sequencing data using breseq. in *Engineering and Analyzing Multicellular*

Systems 165–188 (Humana Press, 2014).
66. Adler, B. A. *et al.* Broad-spectrum CRISPR-Cas13a enables efficient phage genome editing. *Nat. Microbiol.* **7**, 1967–1979 (2022).
67. Katoh, K. & Standley, D. M. MAFFT multiple sequence alignment software version 7: improvements in performance and usability. *Mol. Biol. Evol.* **30**, 772–780 (2013).
68. Nguyen, L.-T., Schmidt, H. A., von Haeseler, A. & Minh, B. Q. IQ-TREE: A fast and effective stochastic algorithm for estimating maximum-likelihood phylogenies. *Mol. Biol. Evol.* **32**, 268–274 (2015).
69. Letunic, I. & Bork, P. Interactive Tree Of Life (iTOL) v5: an online tool for phylogenetic tree display and annotation. *Nucleic Acids Res.* **49**, W293–W296 (2021).
70. Zhou, W. *et al.* Structure of the Human cGAS-DNA Complex Reveals Enhanced Control of Immune Surveillance. *Cell* **174**, 300-311.e11 (2018).
71. Kabsch, W. XDS. *Acta Crystallogr. Sect. D Biol. Crystallogr.* **66**, 125–132 (2010).
72. Evans, P. R. & Murshudov, G. N. How good are my data and what is the resolution? *Acta Crystallogr. Sect. D Biol. Crystallogr.* **69**, 1204–1214 (2013).
73. Mirdita, M. *et al.* ColabFold: making protein folding accessible to all. *Nat. Methods* **19**, 679–682 (2022).
74. Emsley, P. & Cowtan, K. Coot : model-building tools for molecular graphics. *Acta Crystallogr. Sect. D Biol. Crystallogr.* **60**, 2126–2132 (2004).
75. Liebschner, D. *et al.* Macromolecular structure determination using X-rays, neutrons and electrons: recent developments in Phenix. *Acta Crystallogr. Sect. D, Struct. Biol.* **75**, 861–877 (2019).
76. Chen, V. B. *et al.* MolProbity: all-atom structure validation for macromolecular crystallography. *Acta Crystallogr. D. Biol. Crystallogr.* **66**, 12–21 (2010).
77. Karplus, P. A. & Diederichs, K. Linking crystallographic model and data quality. *Science* **336**, 1030–3 (2012).
78. Weiss, M. S. Global indicators of X-ray data quality. *J. Appl. Crystallogr.* **34**, 130–135 (2001).

Data Availability

Data that support the findings of this study are available within the article and its Supplementary Tables. IMG/MGV accessions, protein sequences and nucleotide sequences appear in Supplementary Tables 8–14. Coordinates and structure factors of cbTad1–1″–3′-gcADPR, SPO1 Tad2 apo, SPO1 Tad2–1″–3′-gcADPR, SPO1 Tad2–1″–2′-gcADPR and Had1 have been deposited in the PDB under the accession codes 8SMD, 8SME, 8SMF, 8SMG and 8TTO respectively. The genome sequences of phages SPO1L1-SPO1L5 and SPbetaL1-SPbetaL8 have been deposited with GenBank under accession codes OQ921336-OQ921348, respectively. Source data are available for all the main figures and for extended data figures 2,3,4,5,6,7 and 9.

Acknowledgements

We thank the Sorek laboratory members for comments on the manuscript and fruitful discussion. We also thank Y. Peleg and S. Albeck from the Center for Structural Proteomics within the Weizmann Institute of Science for assistance with protein expression, Y. Fridmann-Sirkis from the Life Sciences Core Facilities of the Weizmann Institute for help with SPR analysis, and H. Keren-Shaul and D. Pilzer from the Life Sciences Core Facilities of the Weizmann Institute for help with PacBio sequencing. R.S. was supported,

in part, by the European Research Council (grant no. ERC-AdG GA 101018520), Israel Science Foundation MAPATS Grant 2720/22), the Deutsche Forschungsgemeinschaft (SPP 2330, Grant 464312965), the Ernest and Bonnie Beutler Research Program of Excellence in Genomic Medicine, and the Knell Family Center for Microbiology. E.Y. is supported by the Clore Scholars Program, and, in part, by the Israeli Council for Higher Education (CHE) via the Weizmann Data Science Research Center. P.J.K. was supported, in part, by the Pew Biomedical Scholars programme and The Mathers Foundation. S.J.H. is supported through a Cancer Research Institute Irvington Postdoctoral Fellowship (no. CRI3996). X-ray data were collected at the Northeastern Collaborative Access Team beamlines 24-ID-C and 24-ID-E (P30 GM124165), and used a Pilatus detector (S10RR029205), an Eiger detector (S10OD021527) and the Argonne National Laboratory Advanced Photon Source (DE-AC02-06CH11357), and at beamline 8.2.1 of the Advanced Light Source, a US DOE Office of Science User Facility under contract no. DE-AC02-05CH11231 and supported in part by the the Howard Hughes Medical Institute, the ALS-ENABLE program, and the NIGMS grant P30 GM124169-01.

Author Contribution

The study was conceptualized and designed by E.Y., A. Leavitt and R.S. E.Y. built and executed the computational pipeline and analyzed the data. A. Leavitt isolated the phages and conducted all the *in vivo* experiments unless stated otherwise. A. Lu and P.J.K. preformed the structural analysis of Tad1 and Tad2. A.E.R. and P.J.K. determined and analyzed the structure of Had1. C.A. and G.A. preformed the biochemical experiments with cell lysates and led the mechanistic characterization of the Tad2 activity. I.O. designed and conducted all the phage knock in experiments and the knockout of *gad2* from phage SPbetaL7. J.G. designed and generated the knock down clones. DNA cleavage experiments were performed by S.P.A., S.E.M., and P.J.K. S.J.H. helped with the structural analysis, characterization of the Tad2 activity, and analysis of Had1 oligomerization. The study was supervised by G.A. and R.S. The manuscript was written by E.Y. and R.S. All authors contributed to editing the manuscript and support the conclusions.

Competing Interests

R.S. is a scientific cofounder and advisor of BiomX and Ecophage. The rest of the authors declare no competing interests.

Extended Data Figure Legends

Extended Data Figure 1. Genome comparisons of phages from the SPbeta and SBSphiJ groups. Genome comparison of (a) eleven phages from the SPbeta group and (b) eight phages from the SBSphiJ group. Amino acid sequence similarity is marked by grey shading. Genome similarity was visualized using clinker[38].

Extended Data Figure 2. Phages from the same family are differentially sensitive to bacterial defense systems. Results of phage infection experiments with (a) eleven phages of the SPbeta group, (b) six phages of the SPO1 group, and (c) eight phages of the SBSphiJ group. Data represent plaque-forming units per ml (PFU/ml) of phages infecting control cells ("no system"), and cells expressing the respective defense systems. Shown is the average of three technical replicates, with individual data points overlaid. The

Thoeris and Hachiman data presented here are the same as those presented in Figures 3b and 5b, respectively.

Extended Data Figure 3. Gad1 proteins inhibit Gabija mediated defense. (a) Multiple sequence alignment of the original Gad1 from phage phi3T and five Gad1 homologs that were chosen for experimental verification. Conserved residues are in purple. (b) Results of phage infection experiments with eleven phages of the SPbeta group. Data represent plaque-forming units per ml (PFU/ml) of phages infecting control cells ("no system"), cells expressing the Gabija system ("Gabija"), and cells co-expressing the Gabija system and a Gad1 homolog. Shown is the average of three technical replicates, with individual data points overlaid. The SPbeta data presented here are the same as those presented in Figure 2d.

Extended Data Figure 4. Gad2 inhibits Gabija mediated defense. (a) Phylogeny and distribution of Gad2 homologs. Homologs that were tested experimentally are indicated on the tree by cyan diamonds. (b) An Alphafold2 model for the structure of Gad2 from phage SPbetaL7. (c) Mutations in the predicted nucleotidyltransferase active site in Gad2 result in loss of anti-defense activity. Data represent plaque-forming units per ml (PFU/ml) of phage SPbeta infecting cells co-expressing the Gabija system and WT or mutated Gad2 from *Brevibacillus laterosporus*, as well control cells expressing neither Gabija nor Gad2 ("Control") and cells expressing the Gabija system without Gad2 ("No Gad2"). Shown is the average of three technical replicates, with individual data points overlaid. (d) SDS-PAGE analysis of Ni-NTA co-purified GajAB with *Shewanella* phage 1/4 Gad1 and *Brevibacillus laterosporus* Gad2 demonstrates that Gad2 does not stably interact with the GajAB complex. Asterisk indicates minor contamination with the *E. coli* protein ArnA. Data are representative of three independent experiments. For gel source data, see Supplementary Figure 1. (e) SDS-PAGE analysis of purified *Brevibacillus laterosporus* Gad2. Asterisk indicates contamination with the *E. coli* protein ArnA. Data are representative of three independent experiments. For gel source data, see Supplementary Figure 1. (f) Biochemical reconstitution of GajAB DNA degradation demonstrates that Gad2 does not directly inhibit GajAB cleavage of a 56-bp target DNA. Data are representative of three independent experiments. For gel source data, see Supplementary Figure 1.

Extended Data Figure 5. Tad2 proteins inhibit Thoeris mediated defense. (a) Multiple sequence alignment of the original Tad2 from phage SPO1, and 5 Tad2 homologs that were chosen for experimental verification. Conserved residues are in purple. Black arrows indicate residues that are involved in 1″–3′ gcADPR binding. (b) Results of phage infection experiments with six phages of the SPO1 group. Data represent plaque-forming units per ml (PFU/ml) of phages infecting control cells ("no system"), cells expressing the Thoeris system ("Thoeris"), and cells co-expressing the Thoeris system and a Tad2 homolog. Shown is the average of three technical replicates, with individual data points overlaid.

Extended Data Figure 6. Tad2 binds 1″–3′ gcADPR. (a) Incubation of Tad2 with 1″–3′ gcADPR in vitro does not yield observable degradation products. Representative HPLC traces of 1″–3′ gcADPR incubated with buffer, Tad2, or with the enzyme Cap-Clip known to cleave diphosphate linkages as a positive control. (b) Size-exclusion chromatography of 1″–3′ gcADPR-bound or apo state Tad2. 1″–3′ gcADPR-bound Tad2 shows a substantial shift compared to Tad2 in the apo state. (c) Surface plasmon resonance binding sensorgrams for Tad2 at five concentrations of 1″–3′ gcADPR. The black lines are the global fits using the instrument's evaluation software. ka = 3.42E+05 ± 5.2E+02 (1/Ms), kd = 0.00798 ±

1142 1E-05 (1/s). (d) Surface plasmon resonance binding sensorgrams for Tad2 at multiple concentrations of
1143 cADPR.
1144
1145 **Extended Data Figure 7. Size-exclusion chromatography of Tad2 and various standards.** Observed
1146 peak demonstrates that Tad2 forms a homomultimer.
1147
1148 **Extended Data Figure 8. Comparison of Tad2 and Tad1 in the apo and ligand-bound states.** (a)
1149 Overview of the crystal structure of SPO1 Tad2 in the apo state in front and top view. (b,c) Overview and
1150 detailed binding pocket views of adenine interactions (left) and ribose/phosphate interactions (right) of
1151 the crystal structures of SPO1 Tad2 in complex with 1″–3′ gcADPR (**b**) or 1″–2′ gcADPR (**c**). (d)
1152 Overview of the crystal structure (PDB: 7UAV) of cbTad1 in the apo state in front view and top view.
1153 (e,f) Overview and detailed binding pocket views of adenine interactions (left) and ribose/phosphate
1154 interactions (right) of the crystal structures of cbTad1 in complex with 1″–3′ gcADPR (**e**) or 1″–2′
1155 gcADPR (**f**, PDB: 7UAW).
1156
1157 **Extended Data Figure 9. Had1 proteins inhibit Hachiman-mediated defense.** (a) Results of phage
1158 infection experiments with eight phages of the SBSphiJ group. Data represent plaque-forming units per
1159 ml (PFU/ml) of phages infecting control cells ("no system"), cells expressing the Hachiman system
1160 ("Hachiman"), and cells co-expressing the Hachiman system and a Had1 homolog. Shown is the average
1161 of three technical replicates, with individual data points overlaid. (b) Structure-guided sequence
1162 alignment of Had1 homologs colored by BLOSUM62 score. (c) SDS-PAGE and (d) SEC-MALS
1163 analysis of purified Had1. Full-length Had1 elutes as a single species that is consistent with a
1164 homodimeric complex (predicted homodimer 12.5 kDa, observed 12.6 kDa). Data are representative of
1165 three independent experiments. For gel source data, see Supplementary Figure 1.
1166
1167 **Extended Data Tables**
1168
1169 **Extended Data Table 1. Summary of crystallography data collection, phasing, and refinement**
1170 **statistics.** All datasets were collected from individual crystals. Values in parentheses are for the highest
1171 resolution shell.
1172
1173
1174

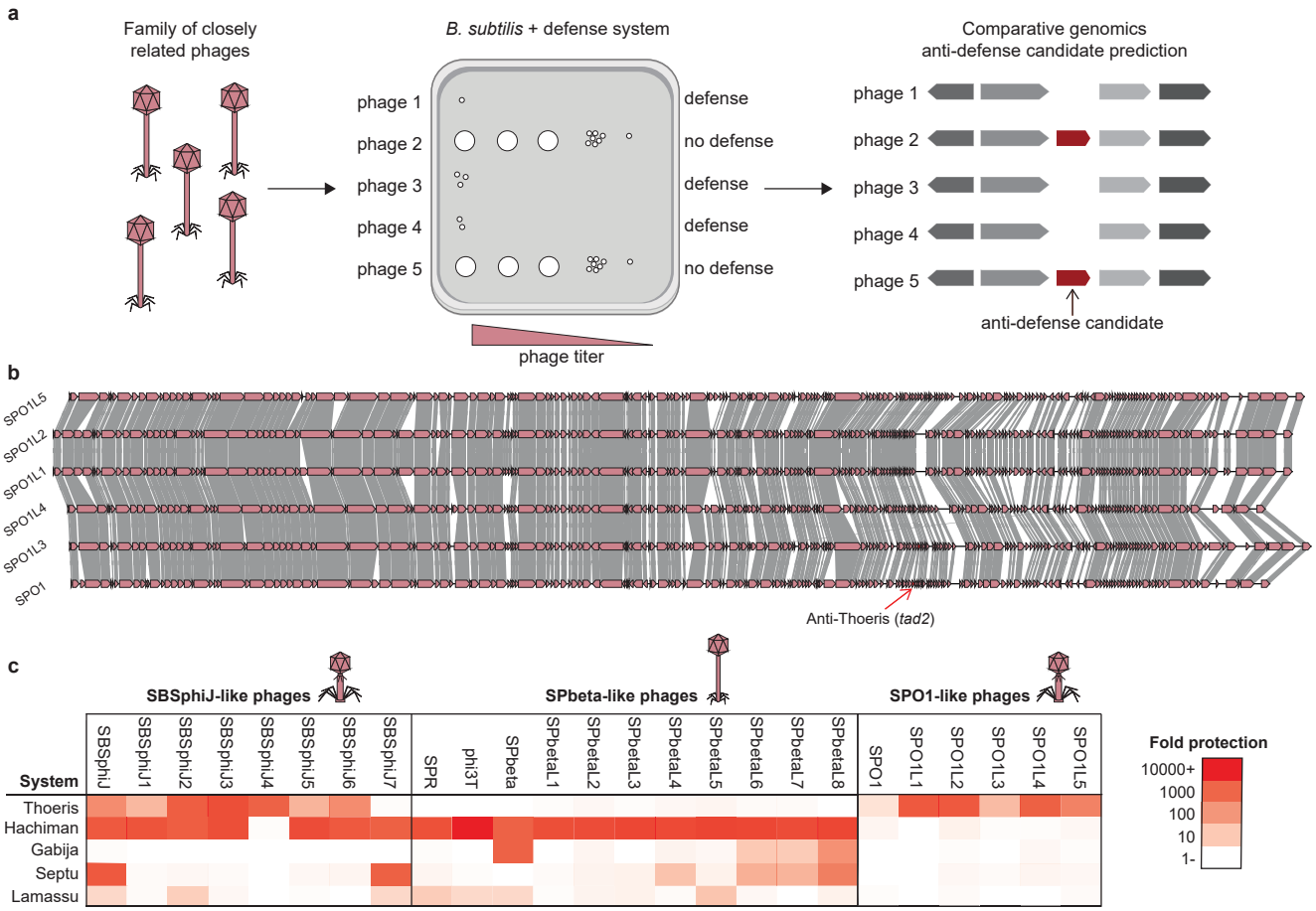
a
Family of closely related phages
B. subtilis + defense system
Comparative genomics anti-defense candidate prediction
phage 1
phage 2
phage 3
phage 4
phage 5
defense
no defense
defense
defense
no defense
phage 1
phage 2
phage 3
phage 4
phage 5
anti-defense candidate
phage titer
b
SPO1L5
SPO1L2
SPO1L1
SPO1L4
SPO1L3
SPO1
Anti-Thoeris (tad2)
c
SBSphiJ-like phages
SPbeta-like phages
SPO1-like phages
System
SBSphiJ
SBSphiJ1
SBSphiJ2
SBSphiJ3
SBSphiJ4
SBSphiJ5
SBSphiJ6
SBSphiJ7
SPR
phi3T
SPbeta
SPbetaL1
SPbetaL2
SPbetaL3
SPbetaL4
SPbetaL5
SPbetaL6
SPbetaL7
SPbetaL8
SPO1
SPO1L1
SPO1L2
SPO1L3
SPO1L4
SPO1L5
Thoeris
Hachiman
Gabija
Septu
Lamassu
Fold protection
10000+
1000
100
10
1-

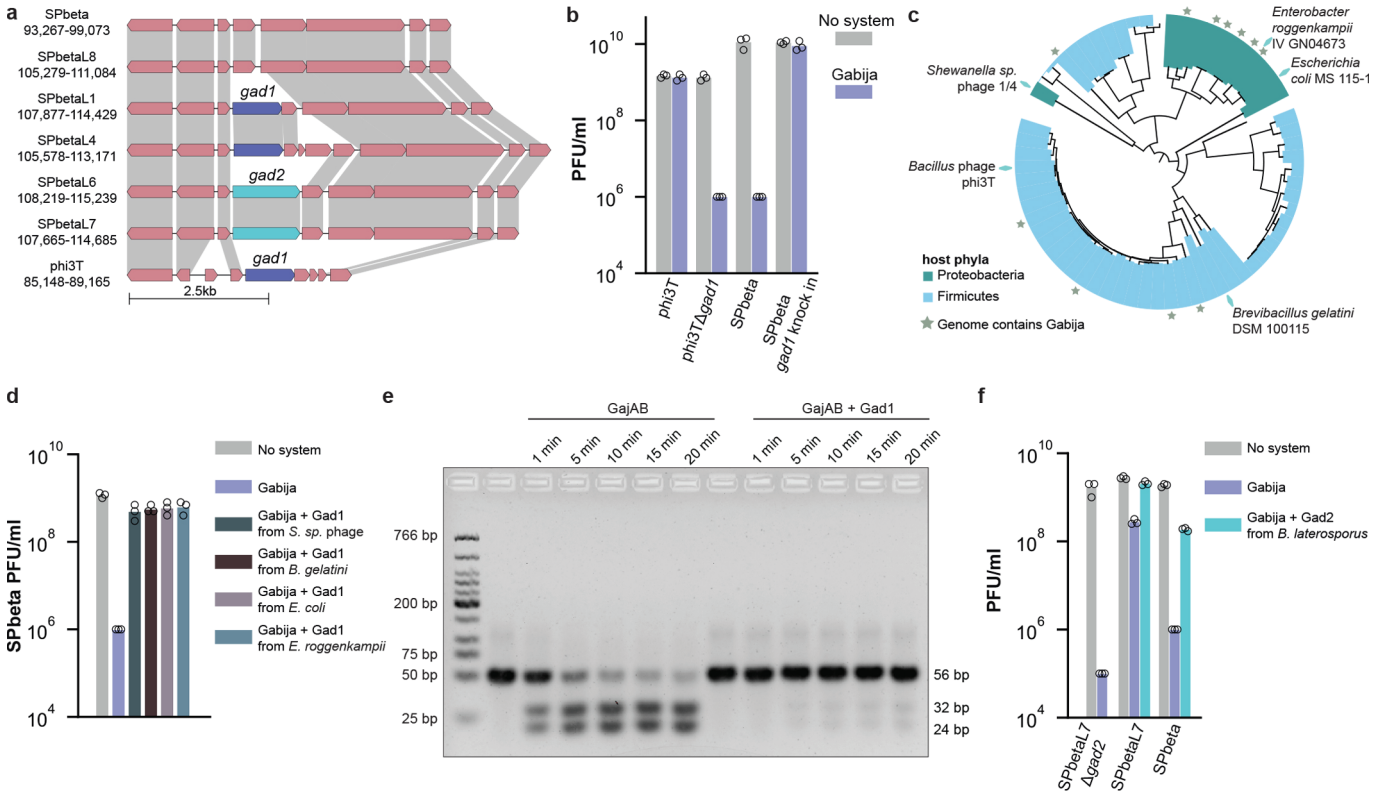
a
SPbeta
93,267-99,073
SPbetaL8
105,279-111,084
SPbetaL1
107,877-114,429
SPbetaL4
105,578-113,171
SPbetaL6
108,219-115,239
SPbetaL7
107,665-114,685
phi3T
85,148-89,165
gad1
gad2
gad1
2.5kb
b
No system
Gabija
PFU/ml
phi3T
phi3TΔgad1
SPbeta
SPbeta gad1 knock in
c
Enterobacter roggenkampii IV GN04673
Escherichia coli MS 115-1
Shewanella sp. phage 1/4
Bacillus phage phi3T
Brevibacillus gelatini DSM 100115
host phyla
Proteobacteria
Firmicutes
Genome contains Gabija
d
SPbeta PFU/ml
No system
Gabija
Gabija + Gad1 from S. sp. phage
Gabija + Gad1 from B. gelatini
Gabija + Gad1 from E. coli
Gabija + Gad1 from E. roggenkampii
e
GajAB
GajAB + Gad1
1 min
5 min
10 min
15 min
20 min
766 bp
200 bp
75 bp
50 bp
25 bp
56 bp
32 bp
24 bp
f
PFU/ml
No system
Gabija
Gabija + Gad2 from B. laterosporus
SPbetaL7 Δgad2
SPbetaL7
SPbeta

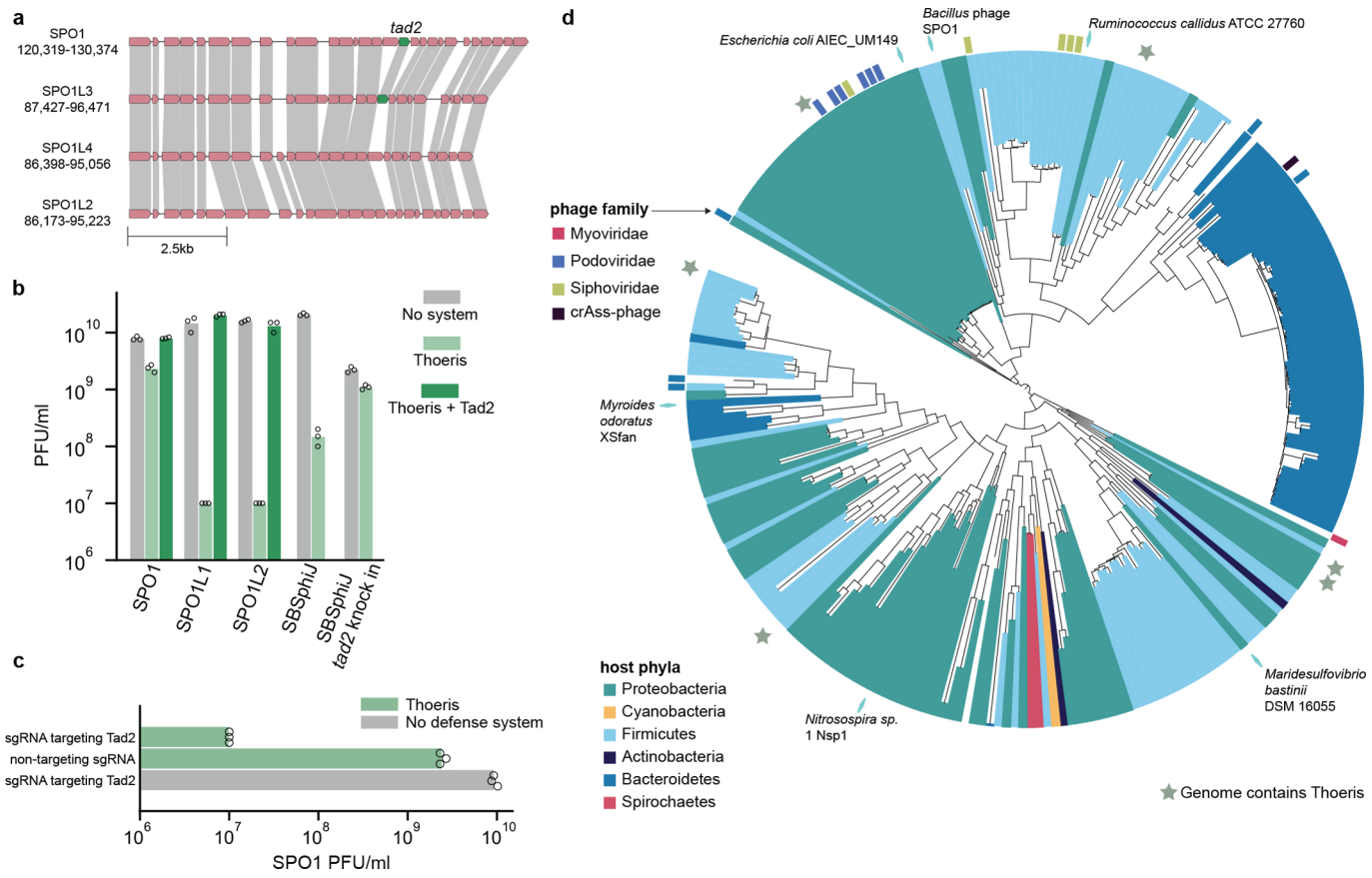
a
SPO1
120,319-130,374
SPO1L3
87,427-96,471
SPO1L4
86,398-95,056
SPO1L2
86,173-95,223
tad2
2.5kb
b
PFU/ml
No system
Thoeris
Thoeris + Tad2
SPO1
SPO1L1
SPO1L2
SBSphiJ
SBSphiJ tad2 knock in
c
Thoeris
No defense system
sgRNA targeting Tad2
non-targeting sgRNA
sgRNA targeting Tad2
SPO1 PFU/ml
d
Escherichia coli AIEC_UM149
Bacillus phage SPO1
Ruminococcus callidus ATCC 27760
phage family
Myoviridae
Podoviridae
Siphoviridae
crAss-phage
Myroides odoratus XSfan
Nitrosospira sp. 1 Nsp1
Maridesulfovibrio bastinii DSM 16055
host phyla
Proteobacteria
Cyanobacteria
Firmicutes
Actinobacteria
Bacteroidetes
Spirochaetes
Genome contains Thoeris

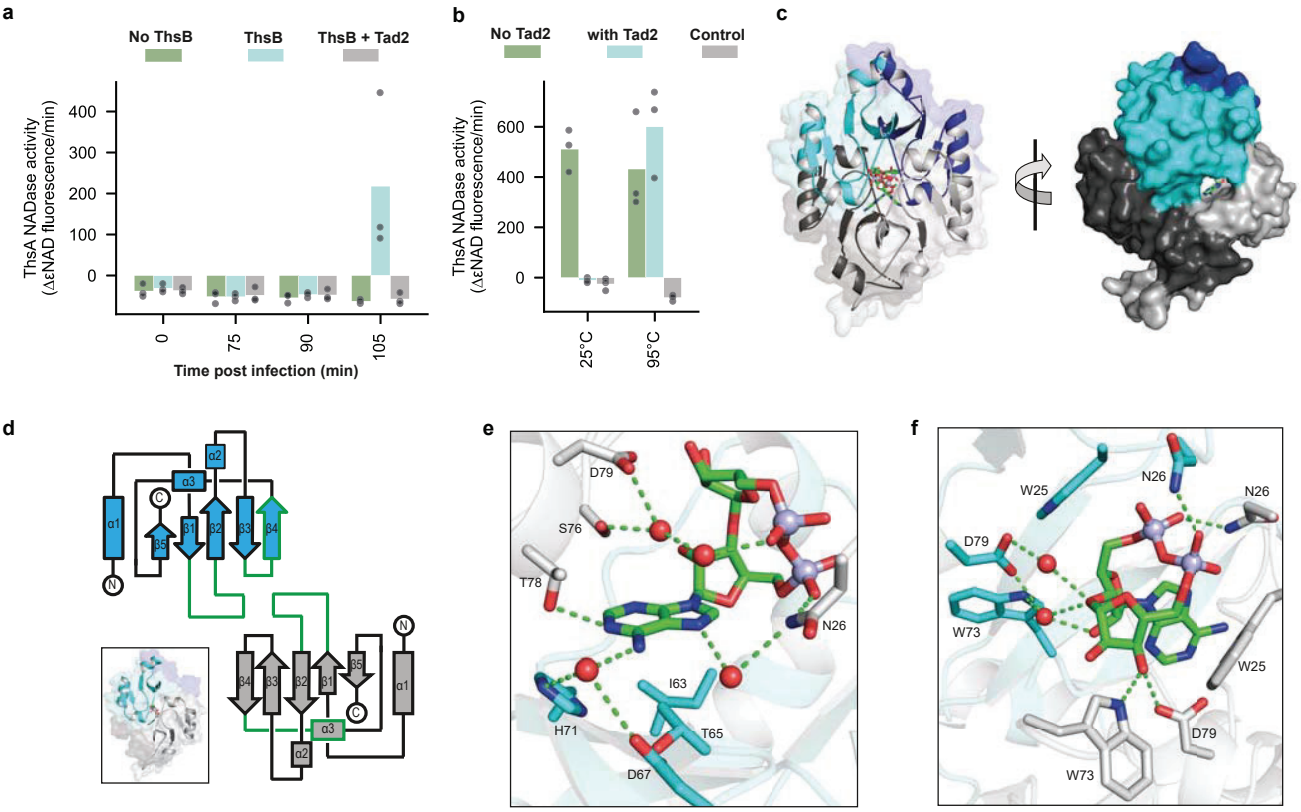
a
No ThsB
ThsB
ThsB + Tad2
ThsA NADase activity
(ΔεNAD fluorescence/min)
400
300
200
100
0
0
75
90
105
Time post infection (min)
b
No Tad2
with Tad2
Control
ThsA NADase activity
(ΔεNAD fluorescence/min)
600
400
200
0
25°C
95°C
c
d
α1
α2
α3
β1
β2
β3
β4
β5
N
C
e
D79
S76
T78
N26
I63
H71
T65
D67
f
W25
N26
N26
D79
W73
W25
D79
W73

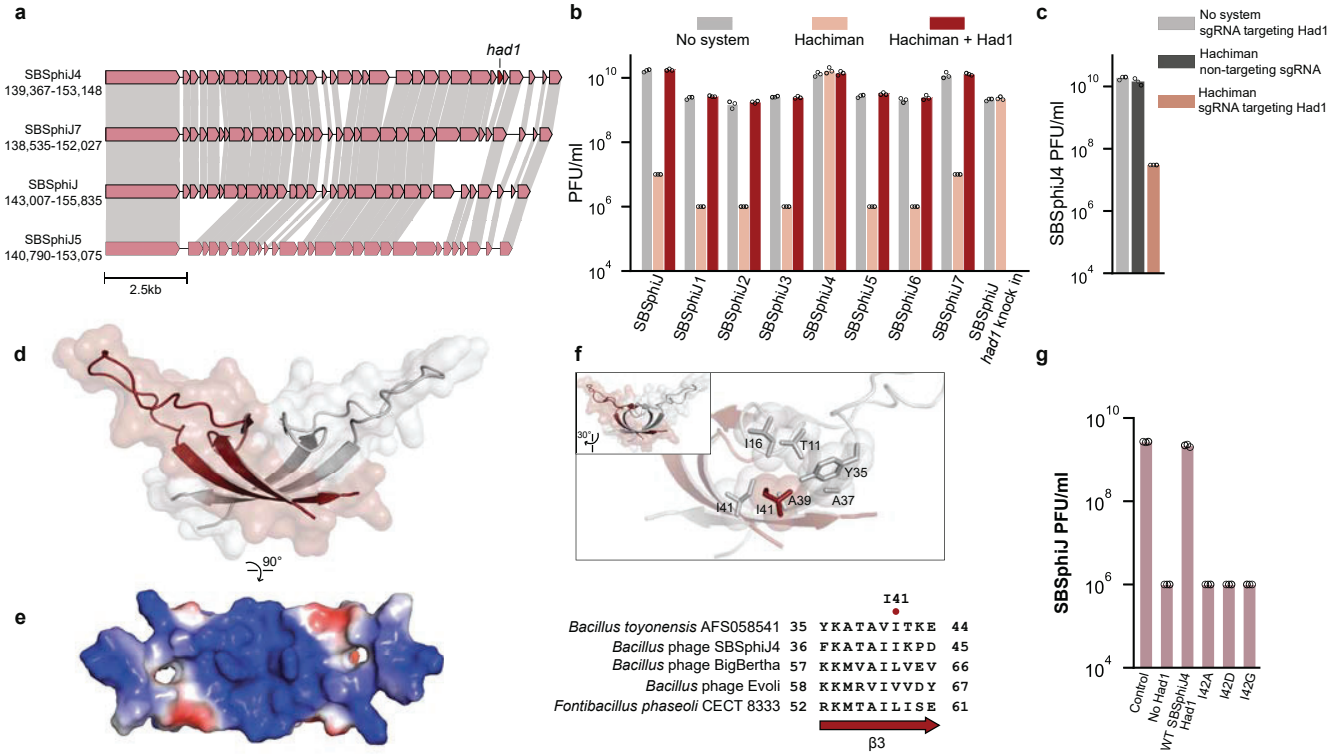
a
had1
SBSphiJ4
139,367-153,148
SBSphiJ7
138,535-152,027
SBSphiJ
143,007-155,835
SBSphiJ5
140,790-153,075
2.5kb
b
No system
Hachiman
Hachiman + Had1
PFU/ml
SBSphiJ
SBSphiJ1
SBSphiJ2
SBSphiJ3
SBSphiJ4
SBSphiJ5
SBSphiJ6
SBSphiJ7
SBSphiJ had1 knock in
c
No system sgRNA targeting Had1
Hachiman non-targeting sgRNA
Hachiman sgRNA targeting Had1
SBSphiJ4 PFU/ml
d
90°
e
f
30°
I16
T11
Y35
I41
I41
A39
A37
I41
Bacillus toyonensis AFS058541 35 YKATAVITKE 44
Bacillus phage SBSphiJ4 36 FKATAIIKPD 45
Bacillus phage BigBertha 57 KKMVAILVEV 66
Bacillus phage Evoli 58 KKMRVIVVDY 67
Fontibacillus phaseoli CECT 8333 52 RKMTAILISE 61
β3
g
SBSphiJ PFU/ml
Control
No Had1
WT SBSphiJ4 Had1
I42A
I42D
I42G

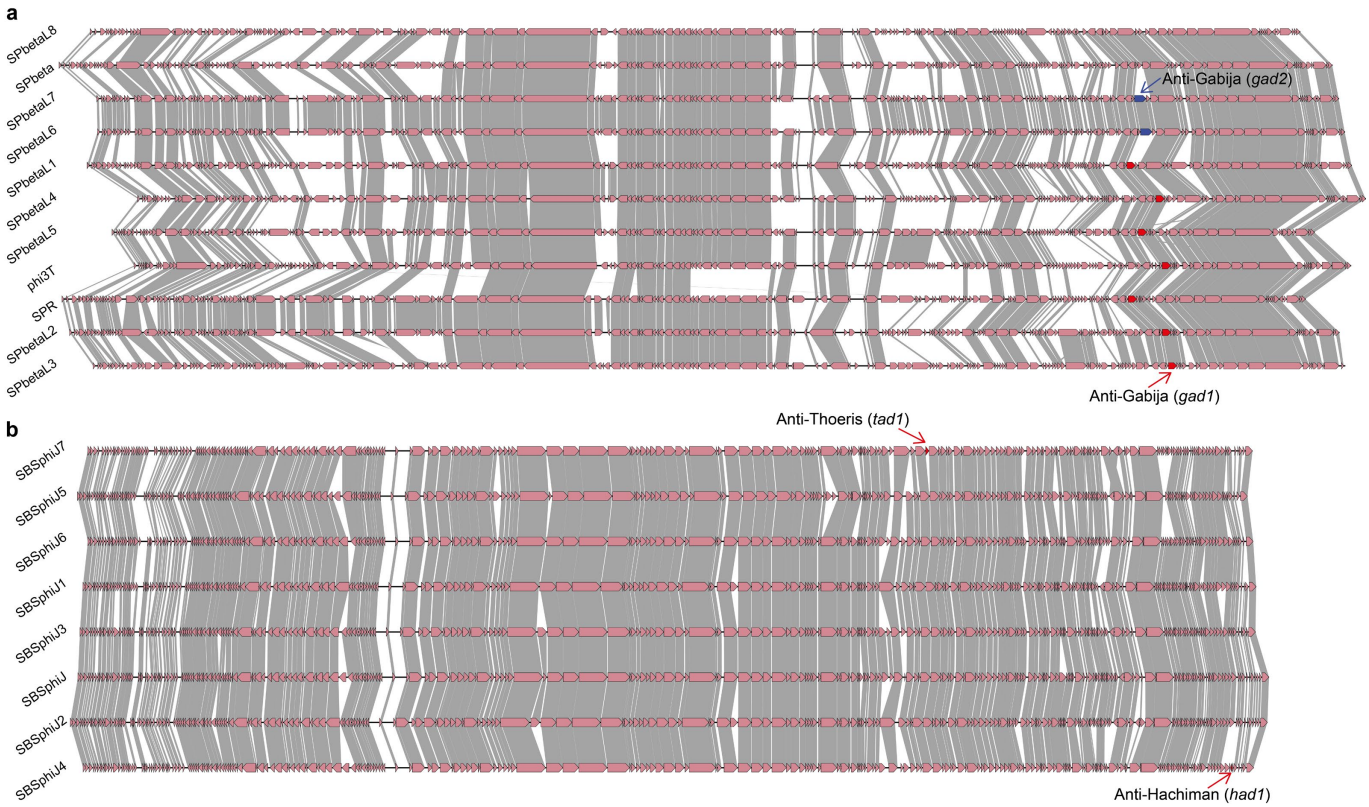

Extended Data Fig. 1

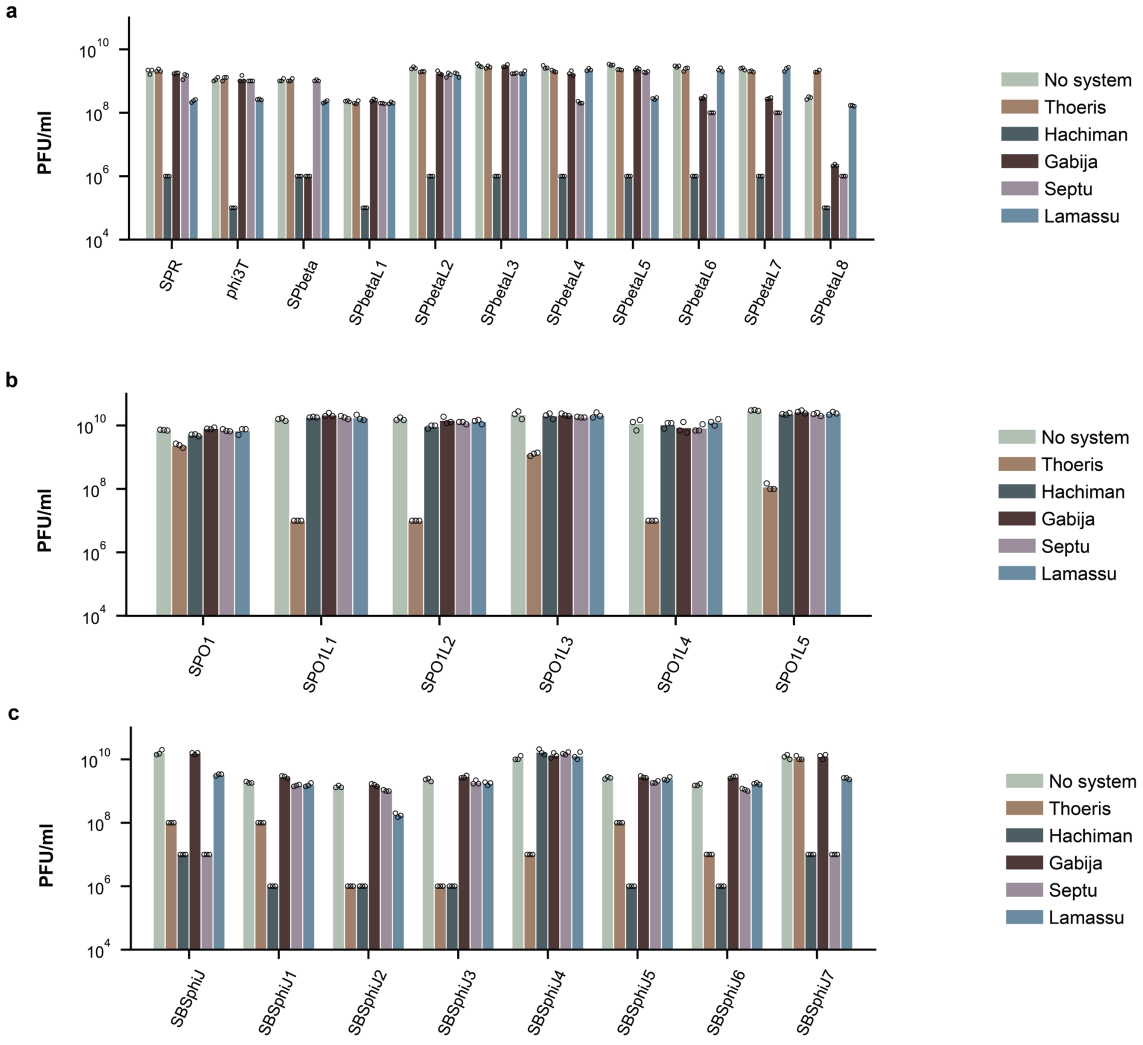

Extended Data Fig. 2

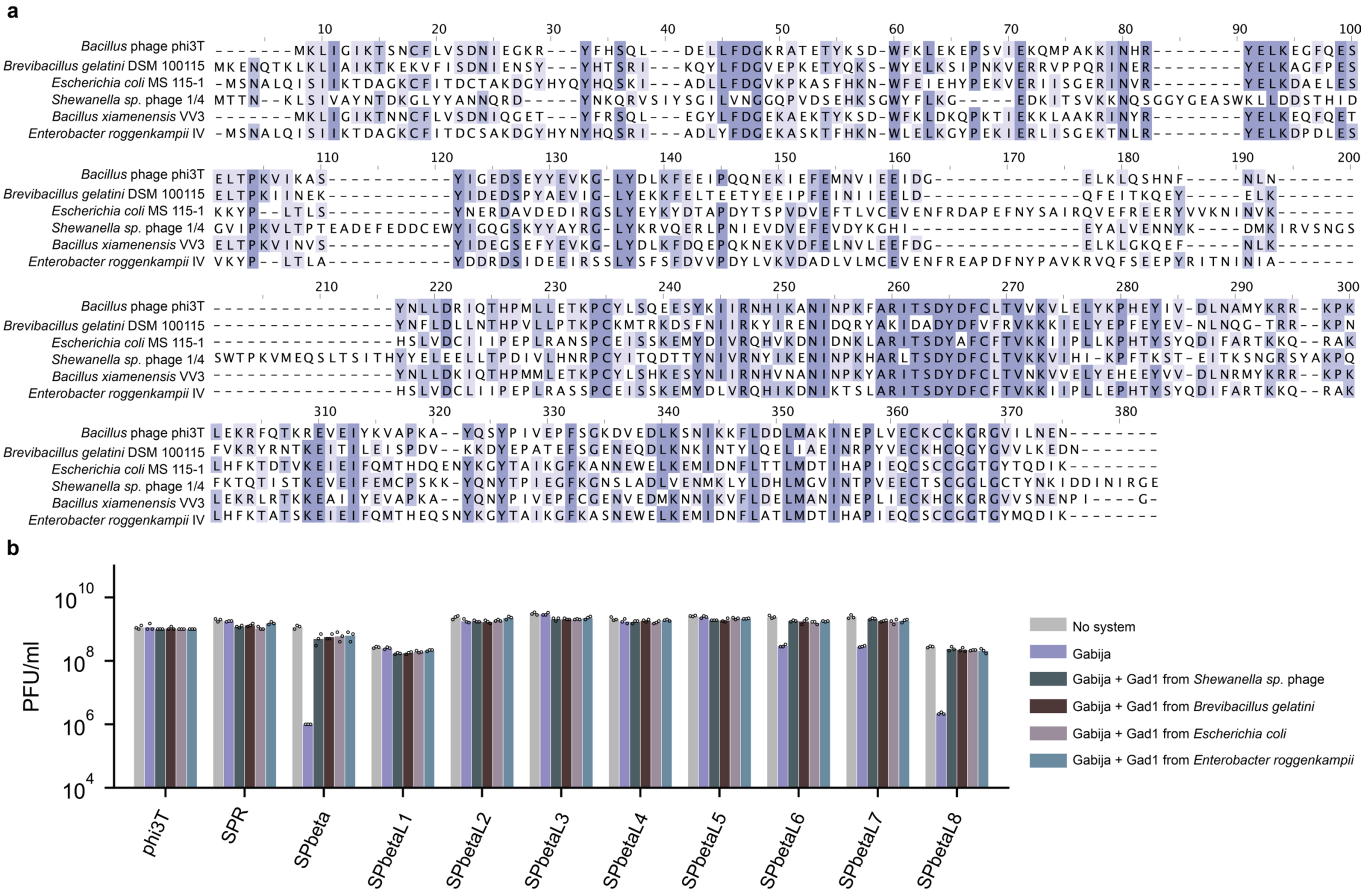

Extended Data Fig. 3

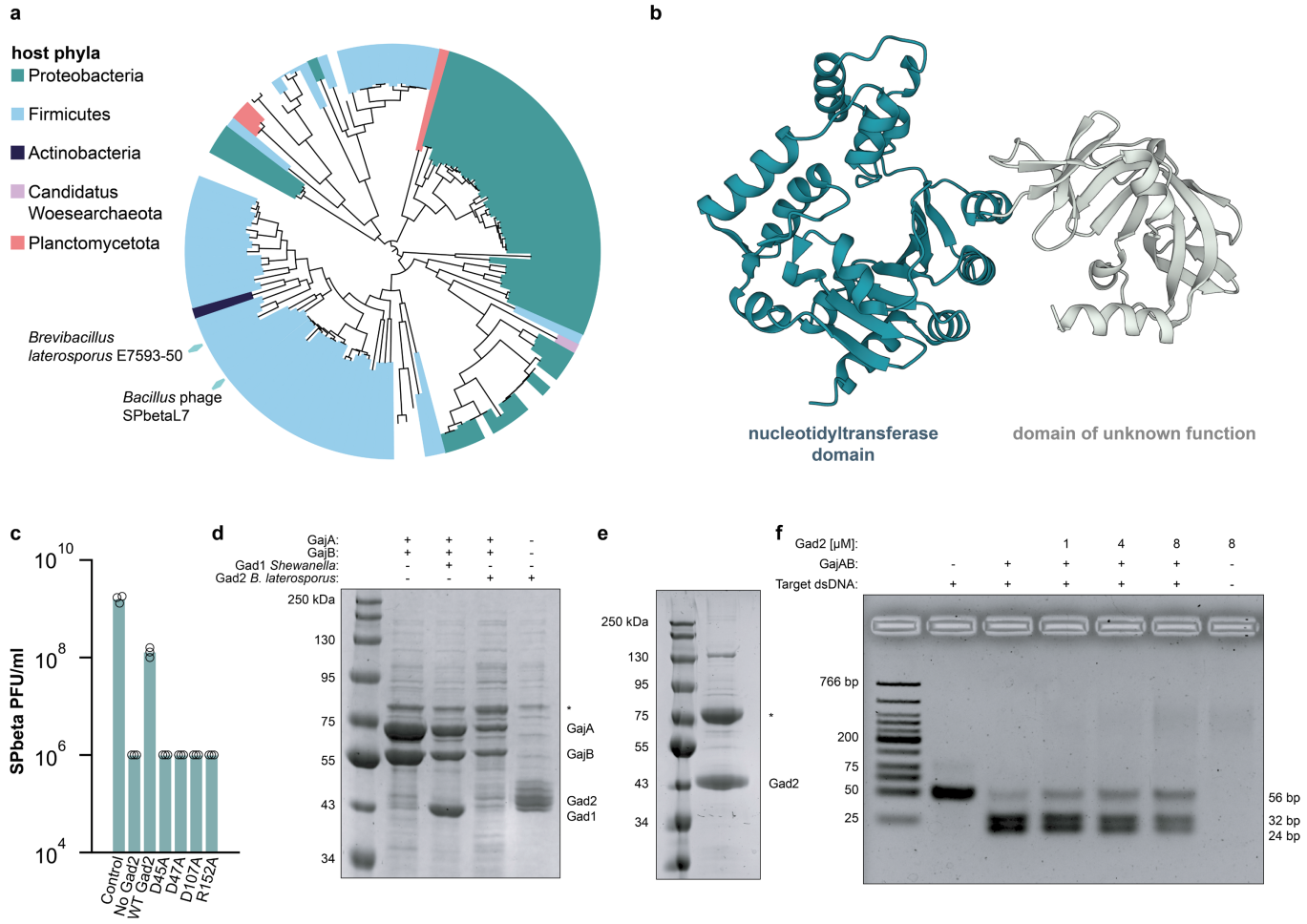

Extended Data Fig. 4

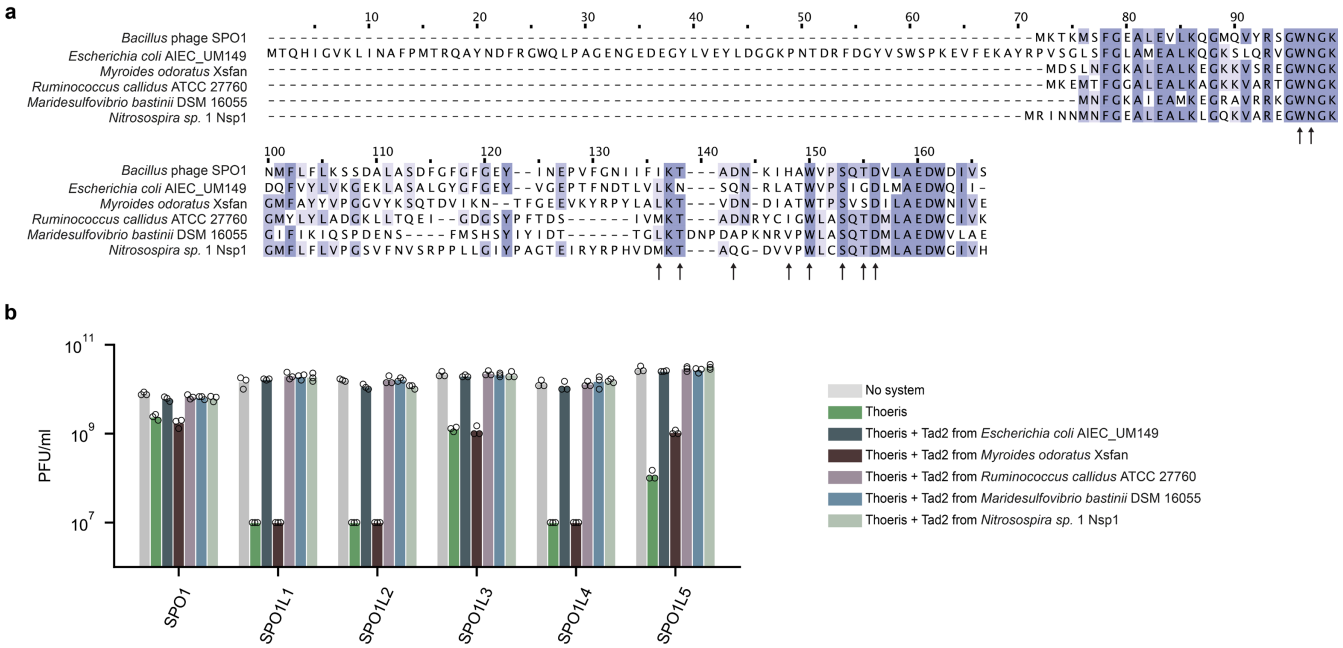

Extended Data Fig. 5

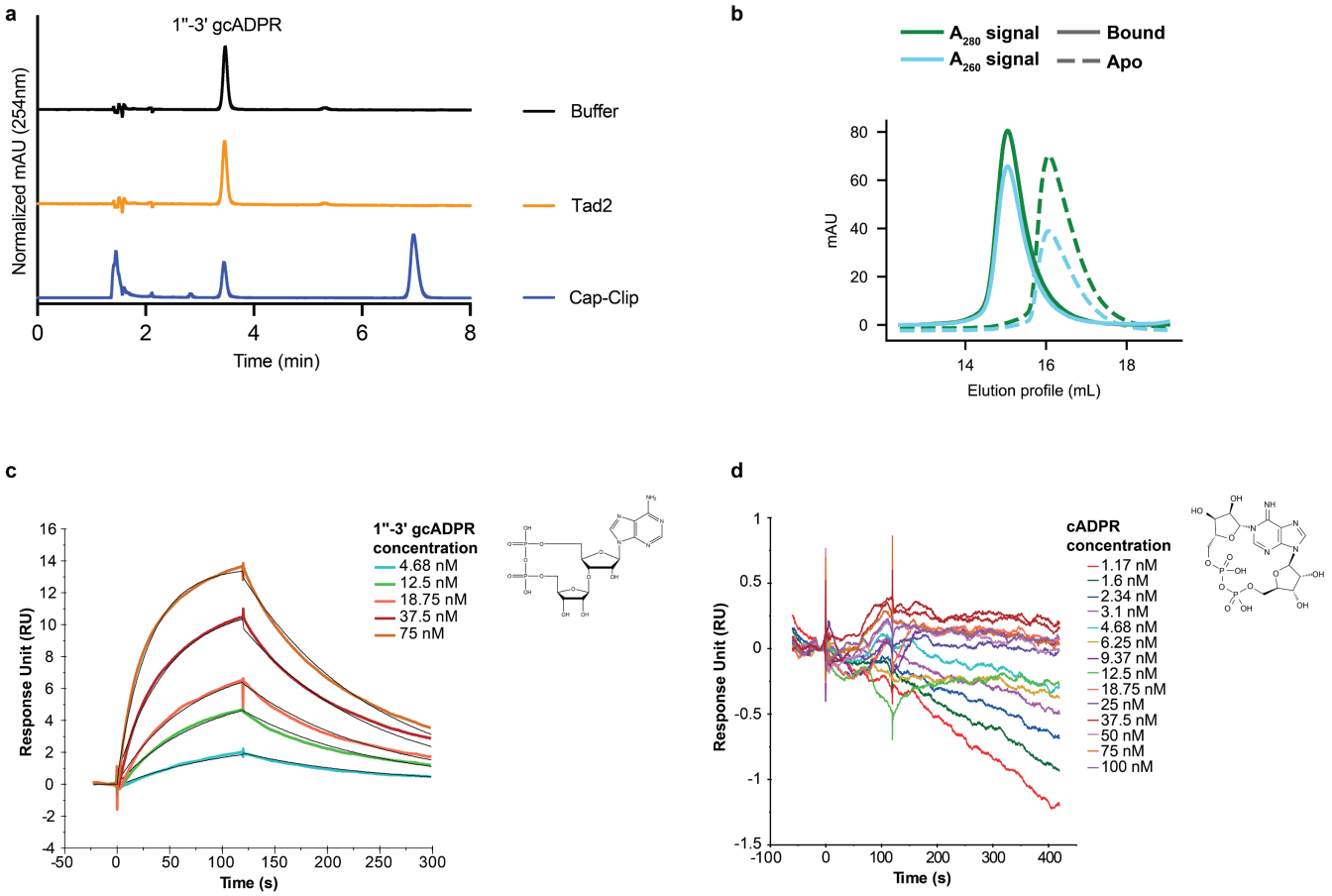

Extended Data Fig. 6

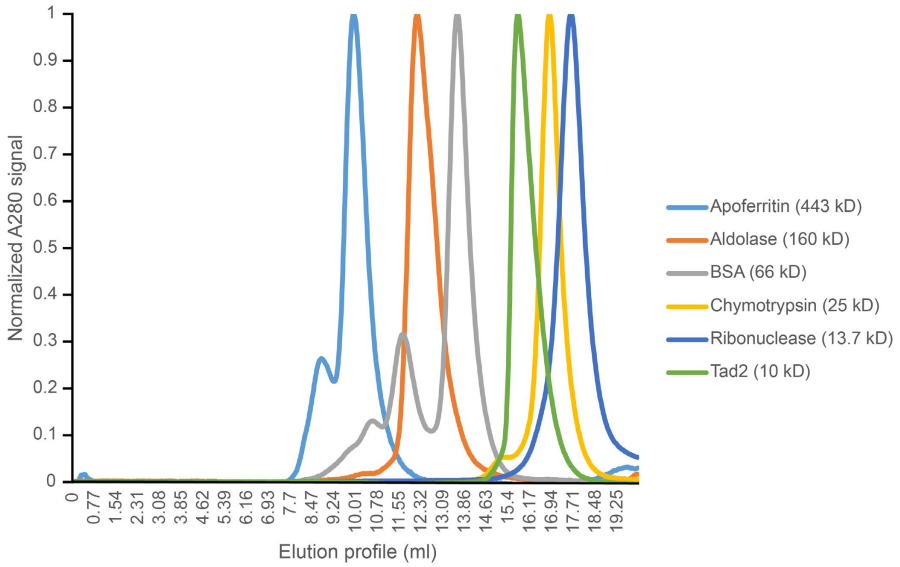

Extended Data Fig. 7

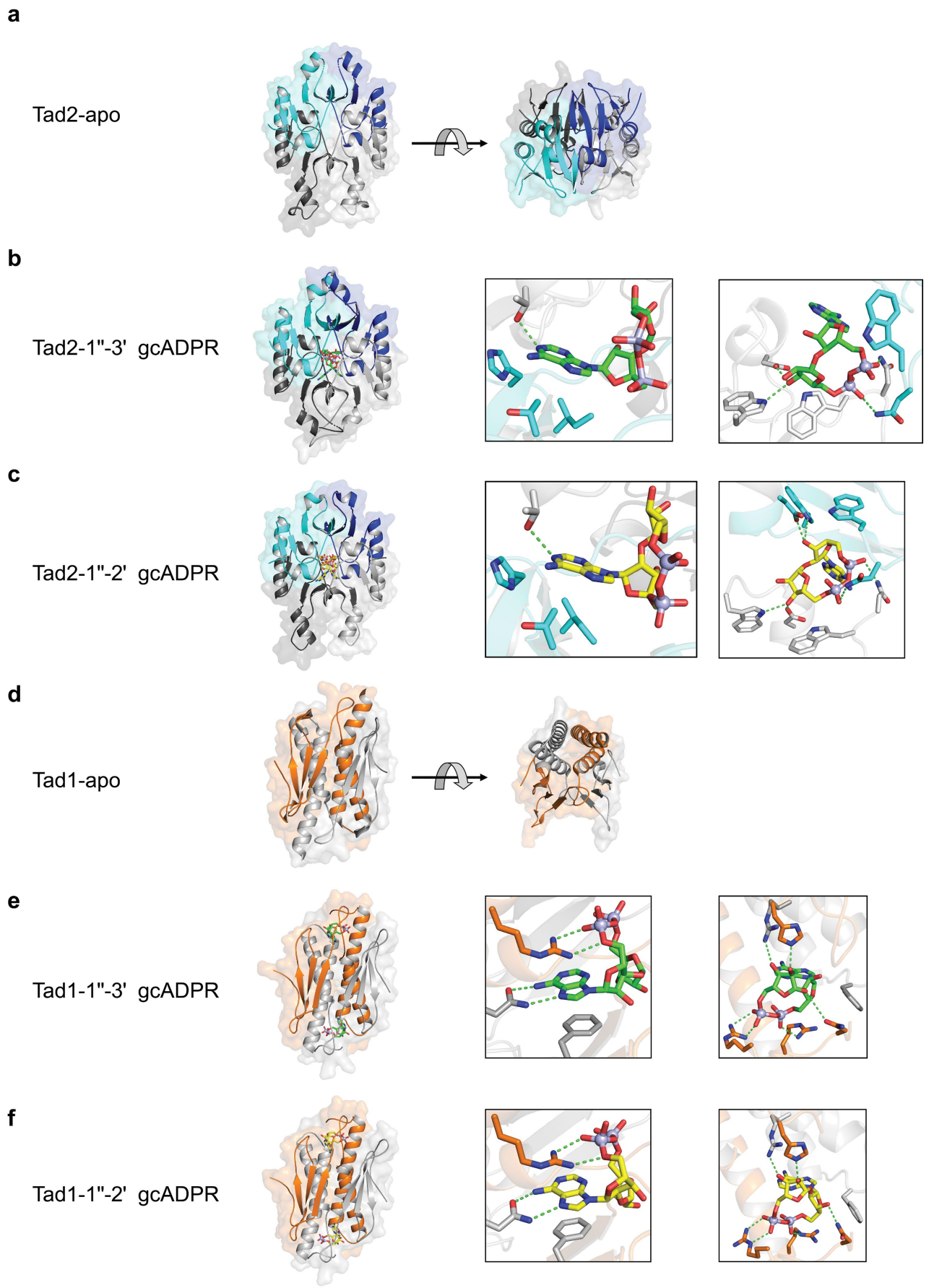

Extended Data Fig. 8

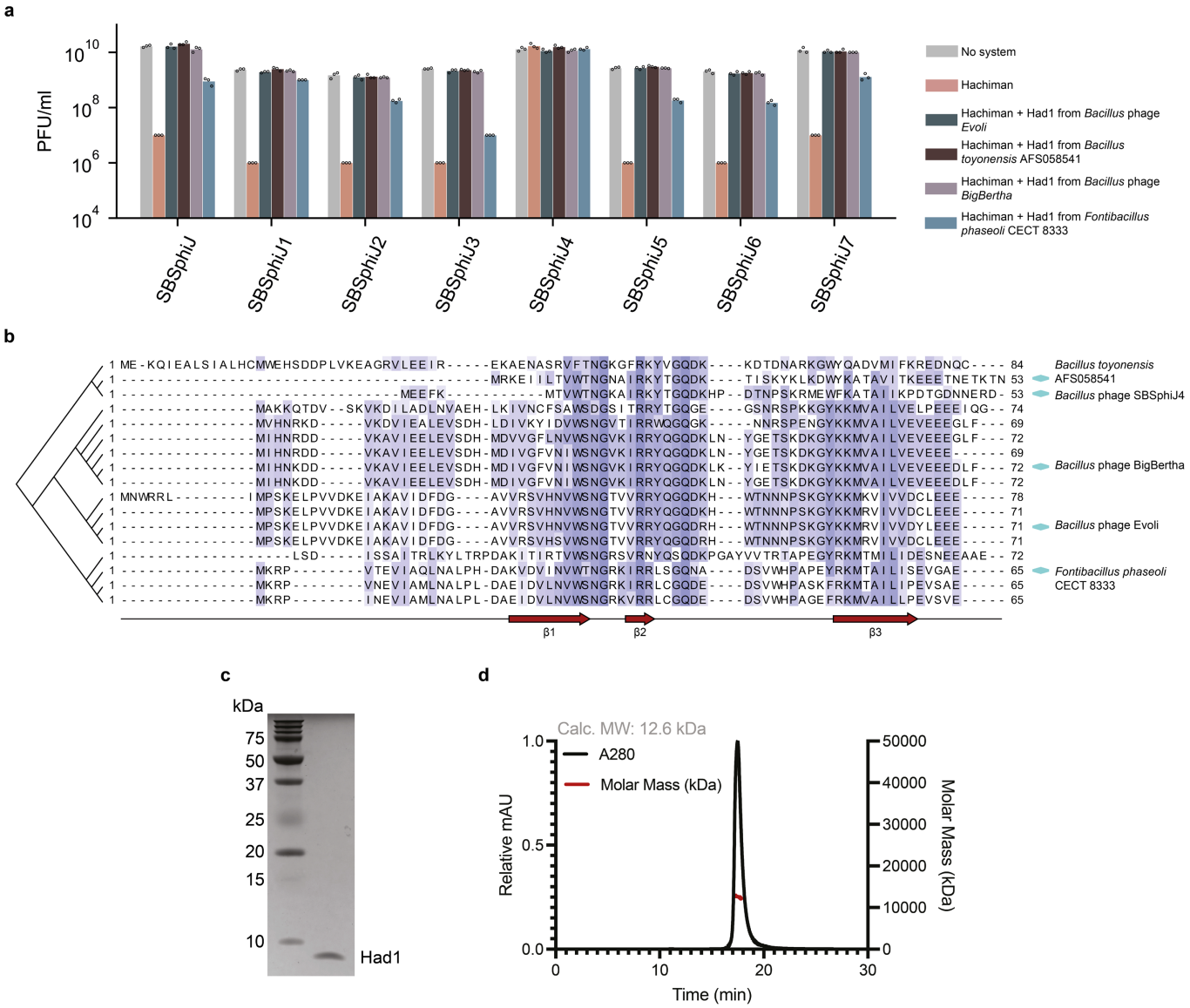

Extended Data Fig. 9

	cbTAD1– 1″–3′ gcADPR **(8SMD)**	SPO1 TAD2– apo **(8SME)**	SPO1 TAD2– 1″–3′ gcADPR **(8SMF)**	SPO1 TAD2– 1″–2′ gcADPR **(8SMG)**	Had1 **(8TTO)**
Data collection					
Space group	P 2_1 3	P 6_3 2 2	C 1 2 1	P 6_3 2 2	P 1
Cell dimensions					
a, *b*, *c* (Å)	95.97, 95.97, 95.97	108.40, 108.40, 74.26	94.39, 82.47, 90.76	108.06, 108.06, 72.36	30.94, 40.18, 45.29
α, β, γ (°)	90.00, 90.00, 90.00	90.00, 90.00, 120.00	90.00, 107.88, 90.00	90.00, 90.00, 120.00	75.22, 89.42, 74.91
Resolution (Å)	42.92–2.10 (2.16–2.10)	46.94–2.36 (2.45–2.36)	46.06–1.75 (1.78–1.75)	39.29–2.10 (2.16–2.10)	37.45-2.00 (2.05-2.00)
R_{pim}	2.5 (69.8)	1.9 (81.5)	5.7 (63.0)	2.2 (71.9)	0.079 (0.684)
I / σ(I)	12.2 (1.0)	19.6 (1.5)	6.5 (1.1)	17.3 (1.5)	4.9 (1.0)
Completeness (%)	99.7 (96.3)	100.0 (100.0)	98.8 (97.1)	100.0 (99.8)	97.3 (95.2)
Redundancy	13.5 (13.3)	27.0 (26.7)	5.2 (4.7)	27.5 (26.8)	1.8 (1.8)
Refinement					
Resolution (Å)	42.92–2.10	46.94–2.36	46.06–1.75	39.29–2.10	37.45-2.00
No. reflections					
Total	236478	298974	344731	414196	24521
Unique	17522	11073	65939	15065	13372
Free	876	1103	1994	1503	1327
R_{work} / R_{free}	20.12 / 23.61	26.29 / 29.87	20.77 / 24.14	22.39 / 24.99	21.53 / 25.54
No. atoms					
Protein	1984 (2 copies)	1281	5054 (8 copies)	1284 (2 copies)	1533
Ligand / ion	70	–	142	35	–
Water	60	2	599	27	172
B-factors					
Protein	61.50	86.46	24.43	72.56	31.07
Ligand / ion	55.31	–	16.62	58.93	–
Water	55.46	59.19	34.43	59.70	36.04
R.m.s. deviations					
Bond lengths (Å)	0.001	0.002	0.004	0.002	0.001
Bond angles (°)	0.433	0.434	0.795	0.463	0.41

Extended Data Table 1

nature portfolio

Corresponding author(s): Gil Amitai, Rotem Sorek

Last updated by author(s): Oct 17, 2023

Reporting Summary

Nature Portfolio wishes to improve the reproducibility of the work that we publish. This form provides structure for consistency and transparency in reporting. For further information on Nature Portfolio policies, see our Editorial Policies and the Editorial Policy Checklist.

Statistics

For all statistical analyses, confirm that the following items are present in the figure legend, table legend, main text, or Methods section.

n/a	Confirmed	
☐	☒	The exact sample size (*n*) for each experimental group/condition, given as a discrete number and unit of measurement
☐	☒	A statement on whether measurements were taken from distinct samples or whether the same sample was measured repeatedly
☒	☐	The statistical test(s) used AND whether they are one- or two-sided *Only common tests should be described solely by name; describe more complex techniques in the Methods section.*
☒	☐	A description of all covariates tested
☒	☐	A description of any assumptions or corrections, such as tests of normality and adjustment for multiple comparisons
☐	☒	A full description of the statistical parameters including central tendency (e.g. means) or other basic estimates (e.g. regression coefficient) AND variation (e.g. standard deviation) or associated estimates of uncertainty (e.g. confidence intervals)
☒	☐	For null hypothesis testing, the test statistic (e.g. *F*, *t*, *r*) with confidence intervals, effect sizes, degrees of freedom and *P* value noted *Give P values as exact values whenever suitable.*
☒	☐	For Bayesian analysis, information on the choice of priors and Markov chain Monte Carlo settings
☒	☐	For hierarchical and complex designs, identification of the appropriate level for tests and full reporting of outcomes
☒	☐	Estimates of effect sizes (e.g. Cohen's *d*, Pearson's *r*), indicating how they were calculated

Our web collection on statistics for biologists contains articles on many of the points above.

Software and code

Policy information about availability of computer code

Data collection	No software was used for data collection
Data analysis	Cutadapt 2.8, SPAdes 3.14.0, Prodigal 2.6.3, MMseqs2 (release 12-113e3), MAFFT 7.402, IQ-TREE 1.6.5, iTOL24 5, Phenix 1.17, Coot 0.8.9, PyMOL 2.3.0, Clinker 1.78, XDS release 2010, aimless release 2013

For manuscripts utilizing custom algorithms or software that are central to the research but not yet described in published literature, software must be made available to editors and reviewers. We strongly encourage code deposition in a community repository (e.g. GitHub). See the Nature Portfolio guidelines for submitting code & software for further information.

Data

Policy information about availability of data

All manuscripts must include a data availability statement. This statement should provide the following information, where applicable:

- Accession codes, unique identifiers, or web links for publicly available datasets
- A description of any restrictions on data availability
- For clinical datasets or third party data, please ensure that the statement adheres to our policy

Data that support the findings of this study are available within the article and its Supplementary Tables. IMG/MGV accessions, protein sequences and nucleotide sequences appear in Supplementary Tables 8–14. Coordinates and structure factors of cbTad1–1′′–3′-gcADPR, SPO1 Tad2 apo, SPO1 Tad2–1′′–3′-gcADPR, SPO1 Tad2–1′′–2′-gcADPR and Had1 have been deposited in the PDB under the accession codes 8SMD, 8SME, 8SMF, 8SMG and 8TTO respectively. The genome

sequences of phages SPO1L1-SPO1L5 and SPbetaL1-SPbetaL8 have been deposited with GenBank under accession codes OQ921336-OQ921348, respectively. Source data are available for all the main figures and for extended data figures 2,3,4,5,6,7 and 9.

Research involving human participants, their data, or biological material

Policy information about studies with human participants or human data. See also policy information about sex, gender (identity/presentation), and sexual orientation and race, ethnicity and racism.

Reporting on sex and gender	Not applicable
Reporting on race, ethnicity, or other socially relevant groupings	Not applicable
Population characteristics	Not applicable
Recruitment	Not applicable
Ethics oversight	Not applicable

Note that full information on the approval of the study protocol must also be provided in the manuscript.

Field-specific reporting

Please select the one below that is the best fit for your research. If you are not sure, read the appropriate sections before making your selection.

☒ Life sciences ☐ Behavioural & social sciences ☐ Ecological, evolutionary & environmental sciences

For a reference copy of the document with all sections, see nature.com/documents/nr-reporting-summary-flat.pdf

Life sciences study design

All studies must disclose on these points even when the disclosure is negative.

Sample size	Experiments were performed in triplicates without prior sample size calculation (unless mentioned otherwise), as is standard for such experimental designs.
Data exclusions	No data were excluded from the analyses.
Replication	Experiments were performed in triplicates. No failed replications occurred.
Randomization	X-ray crystal structures were refined using a randomly selected set of R-free reflections.
Blinding	Blinding was not required in this study as data were collected using highly quantitative measures over multiple independent replicates.

Reporting for specific materials, systems and methods

We require information from authors about some types of materials, experimental systems and methods used in many studies. Here, indicate whether each material, system or method listed is relevant to your study. If you are not sure if a list item applies to your research, read the appropriate section before selecting a response.

Materials & experimental systems

n/a	Involved in the study
☒	☐ Antibodies
☒	☐ Eukaryotic cell lines
☒	☐ Palaeontology and archaeology
☒	☐ Animals and other organisms
☒	☐ Clinical data
☒	☐ Dual use research of concern
☒	☐ Plants

Methods

n/a	Involved in the study
☒	☐ ChIP-seq
☒	☐ Flow cytometry
☒	☐ MRI-based neuroimaging

Plants

Seed stocks	Not applicable
Novel plant genotypes	Not applicable
Authentication	Not applicable